



HAL
open science

Laser-induced breakdown spectroscopy imaging for material and biomedical applications: recent advances and future perspectives

Vincent Gardette, Vincent Motto-Ros, César Alvarez Llamas, Lucie Sancey, Ludovic Duponchel, Benoit Busser

► To cite this version:

Vincent Gardette, Vincent Motto-Ros, César Alvarez Llamas, Lucie Sancey, Ludovic Duponchel, et al.. Laser-induced breakdown spectroscopy imaging for material and biomedical applications: recent advances and future perspectives. *Analytical Chemistry*, 2023, 95 (1), pp.49-69. 10.1021/acs.analchem.2c04910 . inserm-03933204

HAL Id: inserm-03933204

<https://inserm.hal.science/inserm-03933204>

Submitted on 10 Jan 2023

HAL is a multi-disciplinary open access archive for the deposit and dissemination of scientific research documents, whether they are published or not. The documents may come from teaching and research institutions in France or abroad, or from public or private research centers.

L'archive ouverte pluridisciplinaire **HAL**, est destinée au dépôt et à la diffusion de documents scientifiques de niveau recherche, publiés ou non, émanant des établissements d'enseignement et de recherche français ou étrangers, des laboratoires publics ou privés.

Laser-induced breakdown spectroscopy imaging for material and biomedical applications: recent advances and future perspectives

*Vincent Gardette^a, Vincent Motto-Ros^a, César Alvarez Llamas^a, Lucie Sancey^b,
Ludovic Duponchel^c, and Benoit Busser^{b,d,e*}*

Affiliations

- a) Université de Lyon, Université Claude Bernard Lyon 1, CNRS, Institut Lumière Matière, Villeurbanne, France
- b) Univ. Grenoble Alpes, Institute for Advanced Biosciences, Inserm U 1209 / CNRS 5309, 38000 Grenoble, France
- c) Univ. Lille, CNRS, UMR 8516 – LASIRE – Laboratoire de Spectroscopie pour Les Interactions, La Réactivité et L'Environnement, Lille, F-59000, France.
- d) Department of laboratory medicine, Grenoble Alpes University Hospital, 38000, Grenoble, France
- e) Institut Universitaire de France, France

*Email: bbusser@chu-grenoble.fr

AUTHOR INFORMATION

*Corresponding Author

Benoit BUSSER

Univ. Grenoble Alpes, Institute for Advanced Biosciences, Inserm U 1209 / CNRS 5309, 38000 Grenoble, France; Department of laboratory medicine, Grenoble Alpes University Hospital, 38000, Grenoble, France; Institut Universitaire de France, France

Orcid# 0000-0002-9425-1577

Email: bbusser@chu-grenoble.fr

Authors

Vincent GARDETTE

Université de Lyon, Université Claude Bernard Lyon 1, CNRS, Institut Lumière Matière,
Villeurbanne, France

Orcid# 0000-0002-8009-9981

Email: vincent.gardette@univ-lyon1.fr

Vincent MOTTO-ROS

Université de Lyon, Université Claude Bernard Lyon 1, CNRS, Institut Lumière Matière,
Villeurbanne, France

Orcid# 0000-0001-6063-5532

Email: vincent.motto-ros@univ-lyon1.fr

Ludovic DUPONCHEL

Univ. Lille, CNRS, UMR 8516 – LASIRE – Laboratoire de Spectroscopie pour Les Interactions,
La Réactivité et L'Environnement, Lille, F-59000, France.

Orcid# 0000-0002-7206-4498

Email: ludovic.duponchel@univ-lille.fr

Lucie SANCEY

Univ. Grenoble Alpes, Institute for Advanced Biosciences, Inserm U 1209 / CNRS 5309, 38000
Grenoble, France

Orcid# 0000-0002-0084-3775

Email: lucie.sancey@univ-grenoble-alpes.fr

César ALVAREZ LLAMAS

Université de Lyon, Université Claude Bernard Lyon 1, CNRS, Institut Lumière Matière,
Villeurbanne, France

Orcid# 0000-0001-7793-7000

Email: cesar.alvarez-llamas@univ-lyon1.fr

Notes

The authors declare no competing financial interest.

CONTEXT

Laser-induced breakdown spectroscopy (LIBS) is a versatile analytical tool for studying the elemental composition of any kind of sample, such as solids, liquids or gases. One of the latest developments in this technique is the ability to use it for elemental imaging, that is to say spatially resolved surface analysis. LIBS imaging is becoming a very attractive and popular technique for the qualitative and/or quantitative spectrochemical characterization of specimens for a wide range of applications. Because of its unique set of intrinsic advantages, LIBS imaging is frequently preferred over competitive and complementary techniques for elemental imaging.

This review recapitulates the technical fundamentals of LIBS imaging and focuses on significant applications that have received the most promising attention and have undergone major advances during the last three years in the industrial, geological and biomedical fields. We also discuss the current limitations that hinder the further development of LIBS imaging, as well as perspectives on the use of LIBS as a part of multimodal imaging strategies, the contribution of chemometrics, and ideas for improving the limits of detection and quantification aspects.

1. Introduction

In the past few years, the application of laser-induced breakdown spectroscopy (LIBS) in microscopic elemental imaging has been steadily increasing. The recent improvement in its performance makes this technology increasingly attractive for many application fields, including biomedical, geological material analysis, and industry¹⁻⁵. In LIBS-based imaging, a laser-induced plasma is generated at different locations of a sample with a pattern covering the region of interest. Such a plasma source allows specific optical responses resulting from the relaxation of atoms and ions excited by the high plasma temperature (~8 000 K) to be elicited^{6,7}. The major advantage of this approach is that it is possible to perform an elemental measurement from a single laser pulse, which simultaneously samples the material (by laser ablation), atomizes and then excites the ablated vapor by heating the plasma. This facilitates unique features of LIBS-based imaging with a series of advantages, including simple instrumentation, operation at ambient pressure and temperature, a fast

operating speed (up to kHz), and an all-optical design, fully compatible with conventional optical microscopy. Such compatibility plays a facilitating role in coupling LIBS imaging with other techniques, such as Raman spectroscopy and/or luminescence. In addition to this technique having table-top instrumentation, it also has valuable analytical figures of merits, such as no restrictions in the detection of light elements, multielemental capabilities, limits of detection (LoDs) in the range of ppm for most of the elements, and microscopic-scale resolution². All these advantages make LIBS imaging very promising, with the potential to become a reference technique for highly sensitive and spatially resolved elemental approaches, with good complementarities with gold standard methods, such as LA-ICP-MS, synchrotron radiation microanalysis (μ XRF), or electron probe microanalysis (EPMA)⁸⁻¹¹.

The possibility of performing spatially rapid microanalytical measurements by LIBS is not new. In fact, this concept was even at the origin of the first developments related to this technique in the early 1960s¹². At that time, LIBS instrumental developments were focused on microanalysis, and several companies, such as Zeiss, developed commercial instruments fairly quickly¹³. However, with the arrival of more robust lasers and the first matrix detectors on the market, the method underwent more significant development. In the late 1990s and early 2000s, a significant number of publications were published demonstrating all the potential of this technique and paving the way for the development of various applications. For example, this technique was applied to quantify cerium in ceramics at the micrometer scale¹⁴, to perform multielemental LIBS imaging at the kHz operating rate to characterize inclusions in steel¹⁵, to analyze large sample surfaces^{16,17}, and to perform 3-dimensional analysis¹⁸. In the early 2010s, the arrival of new intensified charge coupled device (ICCD) detectors, both faster and more sensitive, on the market truly boosted the development of LIBS-based imaging. This period resulted in several important contributions. First, biological tissue imaging was perceived by the LIBS community as a small revolution, as it opened new avenues for the highly coveted biomedical application field¹⁹⁻²¹. Second, the possibility of obtaining megapixel images was also considered a technological breakthrough, allowing LIBS imaging to become one of the most fashionable hyperspectral methods^{7,22,23}. Finally, what is probably the most important contribution is the amount of work employed to make LIBS imaging technology simple, reliable and fast to use. This last contribution was made possible by a number of companies worldwide, which have focused on developing integrated,

reliable and robust instruments, allowing the technique to reach a previously unattainable level of maturity. These developments are of great benefit to the scientific community, which has access to increasingly powerful instruments offering the opportunity to open up an ever-wider field of applications. However, managing a constantly increasing quantity of data is becoming increasingly difficult. The processing of a large quantity of data is a current obstacle to the development of this technique and its application outside of the laboratory. For this reason, we have chosen to focus this review both on the description of the application fields that seem to have the most potential and on data processing, especially the use of chemometrics methods, which undoubtedly represent a main research challenge for the coming years. However, as a prelude, the following section describes the key instrumental aspects for the implementation of LIBS imaging experiments.

2. Insights into LIBS imaging

2.1 Instrumental basics

LIBS requires a laser pulse to be focused on the sample of interest to ablate a small amount of material (usually a fraction of μg or less) and to create a plasma from the vaporized mass. This laser-induced plasma has a typical lifetime of a few microseconds and a temperature in the range of 10 000 K, allowing the excitation of the vast majority of elements, as well as some radicals formed by recombination during the plasma cooling. As shown in figure 1, the light emitted by the plasma (containing the elemental signature of the sample) is collected by different optical elements (i.e., lenses, mirrors, optical fibers) and then analyzed using an optical spectrometer. The intensity of the lines (atomic, ionic and molecular) observed on the emission spectra is directly related to the elemental composition of the sample.

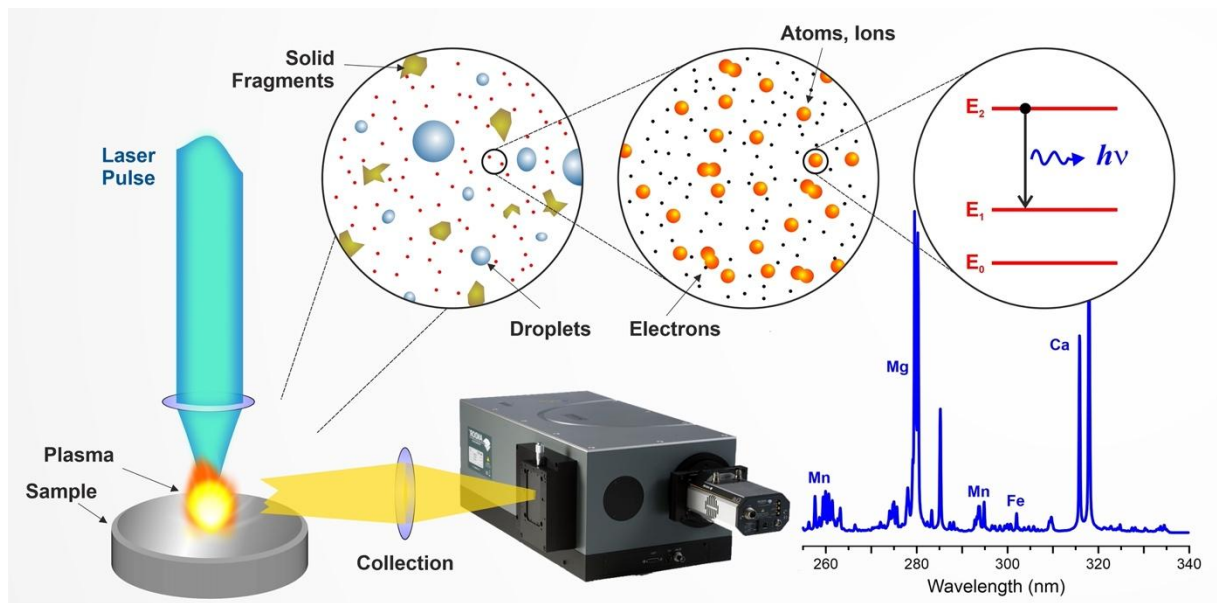


Figure 1. Physical principle of the LIBS technique. Adapted with permission from *Spectrochimica Acta Part B: Atomic Spectroscopy* vol 166, Fabre C., *Advances in Laser-Induced Breakdown Spectroscopy Analysis for Geology: A Critical Review*. p105799 (ref ²⁴). Copyright 2020, with permission from Elsevier.

The principle of LIBS imaging lies in the generation of a series of plasmas at different positions of the sample of interest (Figure 2a)²⁵. Each spectrum is then processed to identify the detected emission lines from the elements of interest and build the corresponding elemental images (Figure 2b-d). For this purpose, the sample is typically positioned on motorized XY stages allowing automated sequences. The lateral resolution or step size (i.e., the distance between consecutive laser shots) then defines the resolution of the final image. In general, the minimal accessible resolution is defined by the crater size. Although it is possible, it is indeed inadvisable to obtain overlaps between consecutive laser shots, since the repeatability of the measurement may be strongly degraded^{26–28}. In addition, it seems worth mentioning that in the vast majority of cases, LIBS imaging instruments rely on the movement of the sample instead of scanning it with a mobile laser beam. It is indeed easier to collect the light emitted from a fixed plasma plume position. However, for specific applications requiring the high-frequency-rate scanning of large-sized sample surfaces (such as online control), moving the laser beam continuously along with the collection system appears to be a valuable strategy^{29–33}.

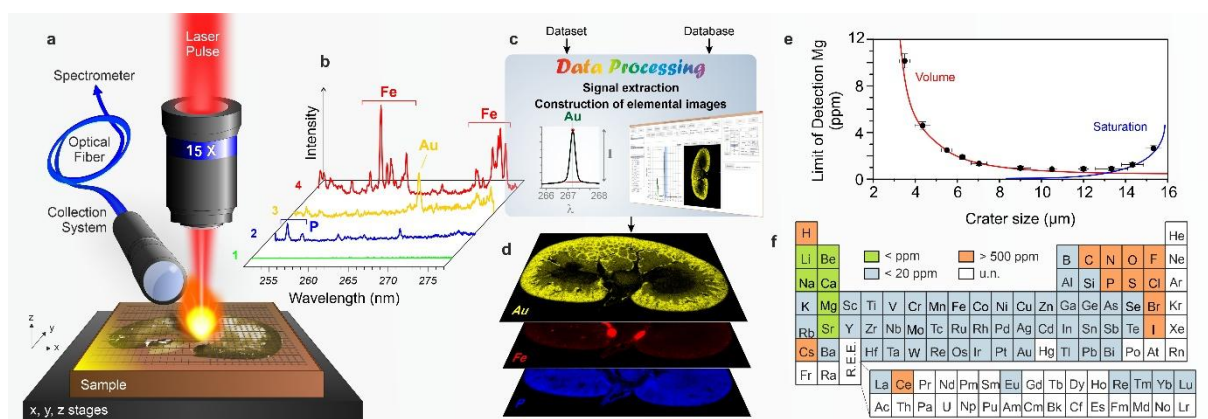


Figure 2: General protocol for LIBS imaging. (a) Schematic view of a micro-LIBS setup showing the major components: the microscope objective used to focus the laser pulse, the motorized platform supporting the sample and the optical detection system connected to the spectrometer via an optical fiber. (b) Example of single-shot emission spectra covering the 250–280 nm spectral range recorded in different regions of a sample (here, a mouse kidney) with the characteristic emission lines of iron (Fe), phosphorous (P) and gold (Au). (c) Data processing step, extraction of the relevant signal and reconstruction of the corresponding elemental images. (d) Example of the relative abundance images of Au (yellow), Fe (red), and P (blue) represented in a false color scale. (e) Evolution of the Mg LoD when reducing the crater size in a configuration using a x15 magnification lens. (f) Estimated values of the relative detection limits obtained in a single pulse configuration (u.n.: unknown). Adapted with permission of MJH Life Sciences, from Gardette, V.; Motto-Ross, V.; Genty, D.; Leprince, M.; Sancey, L.; Pelascini, F.; Busser, B.; Roux, S. LIBS-Based Imaging: Recent Advances and Future Directions. *Spectroscopy* 2020, 35, 34–40. (ref³⁴)

2.2 Instrumental configurations

A very large number of possible instrumental configurations is described in the literature. These have recently been reviewed in several review papers^{2,5}, and only the more important aspects will be discussed in the following. Briefly, LIBS imaging configurations differ by the choice of i) the laser focusing parameters, ii) the laser source and its parameters (wavelength, pulse duration, energy, and pulse frequency or repetition rate), iii) the detection system, composed of spectrometers (monochromator, polychromator, compact, echelle, Pashen Runge) and the detectors (ICCD, linear or matrix CCD/CMOS, photo multiplier, etc.)

2.2.1 Laser focusing

The choice of the focusing system is undoubtedly the most critical one since it will primarily determine the ultimate accessible resolution. Obviously, the shorter the focal length is, the smaller the working distance (WD) and the smaller the crater size. For example, crater diameters smaller than 10 μm may be obtained with a focal length of approximately 15 mm^{6,14}, while obtaining crater diameters of approximately 50 μm is relatively easy with a focal length in the range of 100 mm^{29,35,36}. In a strong focusing configuration (magnification lens higher than x10, WD lower than 15 mm), it may become difficult to couple the plasma light efficiently to the spectrometer due to mechanical constraints². The optics (focusing, collection, etc.) also need to be protected from the ejection of dust and/or particles originating from the ablation process.

Moreover, it is easy to appreciate that a smaller crater implies a lower ablated mass, a smaller number of emitters (excited atoms/ions or molecules) in the plasma, and thus a lower measured signal. In such cases, argon gas can be used to flow the plasma region to obtain higher emission properties as the plasma is thermally insulated and better confined compared to that during ablation in air³⁷⁻³⁹. However, there is always a trade-off between resolution and sensitivity (i.e., the LoD). As an example, the evolution of the magnesium (Mg) LoD as a function of the crater diameter is shown in Figure 2e. This result was obtained using a x15 magnification focusing lens ($f = 13.3 \text{ mm}$) in an argon environment on a reference glass by adjusting the laser pulse energy³⁴. The LoD strongly deteriorates when reducing the crater size and the corresponding ablated volume. Considering the equivalent plasma generation and excitation capabilities of the laser pulse, a change from 10 μm to 1 μm in the crater diameter (as well as the depth) may degrade the LoD by approximately 3 orders of magnitude. This suggests how to obtain a LoD within few % of that obtained in the work of Wang et al., contrasting with the impressive lateral resolution of less than one micrometer⁴⁰. In this experiment, the laser fluence was maintained under the breakdown threshold, and a silver tip was used to locally increase the laser electromagnetic field via localized surface plasmon resonance (LSPR), leading to very localized ablation. Other studies have proposed offsetting such losses with an external addition to the experimental setup^{2,5}. These approaches work, but at the cost of adding experimental constraints. For example,

Ahamer et al. used a femtosecond laser for LIBS imaging, resulting in a high spatial resolution of approximately $6 \mu\text{m}$ ³⁹. To compensate for the sensitivity loss, a strategy with a second pulse for the reheating and excitation of the plume was used by the same laboratory⁴¹.

Although the LIBS technique generally requires very little sample preparation, this step is nonetheless crucial⁴². It is indeed necessary for the sample to be perfectly flat and clean, which is generally achievable through a polishing step. A constraint related to the technique is to guarantee the positioning of the surface plane with respect to the focal plane of the optical system throughout the imaging experiment. This aspect is of uttermost importance, especially when the laser focusing is strong, since the positioning of the sample surface should be controlled at the scale of the Rayleigh length of the beam ($z_R \sim 20 \mu\text{m}$ for a spot diameter of $10 \mu\text{m}$)⁷. Finally, it is important to emphasize that laser ablation is a powerful process. It is indeed accompanied by thermal diffusion through the sample as well as the generation of a shock wave. Both of these effects might cause much more sample deterioration than ablation itself. This is the case for fragile materials in particular, such as thin biological tissue slices. Consequently, to ensure measurement repeatability, the step size (lateral resolution) may be adapted with regard to the sample-induced damage.

2.2.2 Laser source

Regarding the choice of laser, the critical factor for obtaining optimal LIBS imaging results is, above all, the laser shot-to-shot stability (in terms of not only energy but also pulse duration and pointing), considering that any source instability leads to fluctuations in plasma generation and thus also in the collected signal. A laser source with significant shot-to-shot variations degrades the measurement repeatability and thus also the quality of the obtained elemental images. In the case of LIBS imaging, the laser shot-to-shot stability is more critical than in the case of LIBS for bulk or homogeneous sample microanalysis, since in the latter case, it is possible to accumulate a burst of LIBS measurements, which may compensate for some of the laser variability.

The laser wavelength also influences the LIBS signals, as, in some cases, it is difficult to induce the breakdown of the analyzed materials under certain experimental conditions of laser fluence with a specific laser wavelength. Indeed, many materials are transparent in the

visible and near-infrared ranges (with low absorption coefficients at these wavelengths), while very few materials do not absorb in the UV range^{43,44}. In addition, the ablation and plasma dynamics may be drastically different according to the laser wavelength, since plasma plume-laser interaction processes are strongly dependent on the wavelength of the plume, and the plume's predominant physical ionization processes (inverse Bremsstrahlung or photoionization) may vary. For example, plasma has a higher absorptivity in infrared; however, the sample ablation efficiency is higher when using UV lasers. It is initially obvious that the use of UV wavelengths appears more relevant. Unfortunately, this wavelength range is generally only accessible by tripling or quadrupling a Nd:YAG pulse at 1064 nm, resulting in poorer laser emission stability compared with the use of the fundamental wavelength.

In addition, to obtain the best focusing capabilities possible, as close as possible to the diffraction limit, the laser beam quality is important (usually measured as M^2), as well as the diameter of the laser beam before it is focused. The latter can be increased by means of optical elements and/or beam expanders.

2.2.3 Detection system

The choice of detection system (spectrometer and detector) is also a question of compromise. In this case, several parameters, including the spectral resolution, spectral measuring range (multielemental capability), spectrometer brightness (measurement sensitivity), operating speed and cost², must be taken into account to select the appropriate system for a specific application. Unfortunately, a detection system that is able to optimize all these different aspects does not yet exist. For instance, echelle spectrometers have the great advantage of covering a broad spectral range (in general from UV to near-infrared), providing full capabilities in terms of multielemental detection⁴⁵⁻⁴⁸. However, the detection sensitivity (brightness) is rather poor due to the small entrance aperture, typically ϕ 50 μm . In addition, the echelle dispersion may involve the loss of spectral zones located between the diffraction orders. The CCD sensor saturation of one or more emission lines could induce the appearance of "ghost lines" due to CCD blooming. Finally, the acquisition rate is also limited to approximately 1-5 Hz since the detector has to read out the full sensor frame. To combine a high detection sensitivity, high acquisition rate, and broad spectral range, one

could use a Paschen–Runge spectrometer. Such spectrometers are suitable for simultaneous multielemental detection with the use of photomultiplier tubes at slits and/or a combination of linear CCD detectors⁴⁹. With such a configuration, these spectrometers can operate with acquisition speeds up to the kHz range^{15,50,51}. Due to their robustness, Paschen–Runge spectrometers may constitute a relevant choice for industrial applications. However, they are generally costly and bulky apparatuses and should also be ultimately configured once. Czerny–Turner (CT) spectrometers coupled to matrix detectors (CCD, ICCD, EMCCD, etc.) are undoubtedly the most widespread detection systems used for LIBS mapping experiments^{22,23,28,52}. The brightness of such spectrometers is high due to a large entrance slit, and they are generally equipped with 3 to 4 different selectable gratings, ensuring the versatility required for laboratory experiments. In addition, the use of ICCDs as detectors facilitates fast synchronization capabilities, allowing well-resolved temporal measurements to be performed and an acquisition rate of up to 100 Hz⁷. However, the main drawback of CT spectrometers is undeniably their limited spectral detection range, typically with spectral windows from ~20 nm to ~80 nm depending on the required resolution. Several groups have proposed associating several CT spectrometers in the same LIBS experiment^{7,53,54}; however, this results in greater instrumental complexity and associated costs. The use of compact CT spectrometers (Ocean optics, Avantes, etc.) may also be a good approach. Indeed, they have great advantages of affordability and reduced size, which makes their use possible in a multichannel configuration^{29,30,55–57}; however, for certain configurations, the exposition time is not adjustable, which may lead to a higher spectral complexity (all the emission generated during the plasma lifetime is recorded), possibly causing spectral interferences for some emission lines.

Finally, it is important to discuss the operating speed of the detection system (i.e., the number of spectra recorded per second). This is obviously primarily dependent on the laser frequency rate. Currently, we have no difficulty finding lasers on the market between 10 Hz and 1 kHz with enough energy to easily produce laser-induced plasma (>mJ) on almost all types of materials. However, above a certain frequency (typically > 200 Hz), traditional ICCD detectors as well as certain types of CCD sensors can no longer keep up. It is thus necessary to work with faster sensors (including faster phosphors depending on the technology) with

smaller sensitive areas and/or quantum efficiency. In such cases, less light is collected, which leads to a noticeable loss of sensitivity.

2.3 Data processing

One of the challenging tasks in LIBS imaging is undoubtedly data processing. This step basically consists of extracting the relevant information contained in the spectral dataset and representing it in the form of image(s) with spatial distribution for the elements of interest. A detailed section dedicated exclusively to this aspect is proposed below (please refer to section 4). The idea here is to only outline the main difficulties encountered during this phase of data treatment. First, the sample itself may be very complex in terms of composition (with potentially different matrices, as for most geological samples), which leads to different matrix effects that must be taken into account during data processing. Second, it is important to keep in mind that LIBS imaging is based on atomic emission spectroscopy, which may result in a highly complex spectral signal in certain cases. Some elements, such as transition metals (i.e., Fe, Ti, Mo, Ni, ...) indeed have a large number of emission lines in all wavelength domains (from the UV to NIR range). If one or more of these elements are a constituent of a sample, the corresponding spectra will be very dense from a spectral point of view. Consequently, important spectral interferences may occur and affect the signal extraction of other elemental lines, sometimes the most interesting and valuable ones. In addition, in some cases, due to such interference effects, the sensitivity performance may deteriorate significantly, as the number of available lines of the elements of interest is reduced due to interference, which means that the most sensitive line is not always available. In addition, some emission lines present in the spectra may be affected by self-absorption phenomenon (i.e., emitted photons are reabsorbed before they can escape from the plasma), resulting in a reduction in the measured intensity^{58,59}. This effect can be significant if i) there are elements present in high concentrations in the plasma (typically > wt %) and ii) the fundamental level is involved in the line transition. This effect could be advantageous in the case of LIBS imaging because it allows the stretching of the detector

dynamic range in terms of detectable concentration (typically 5 to 6 orders of magnitude, from ppm to tens of percent). Saturation due to self-absorption, involving mainly intense transitions, indeed allows the detection of high concentrations without necessarily saturating the detector. The disadvantage is that the response curve between elemental concentration and line intensity is not linear, at least for high concentrations. These different phenomena increase the dataset complexity, in terms of both wavelength and intensity. Such complexity depends on the elements present in the sample and their amounts, which have to be addressed on a case-by-case basis.

Finally, to top it all, the large number of spectra recorded to generate more than one million pixel images⁷ results in additional difficulties for handling such large datasets. This quantity of data implies the use of little supervised and fast methods for intensity extraction. It seems obviously unthinkable to manually process a million spectra. Today, there are many different processing methodologies that may or may not include an image processing phase. They can be broadly classified into two categories of methods: univariate and multivariate. Specifically, for example, a univariate method potentially uses a single given wavelength to generate an image. On the other hand, a multivariate chemometrics method exploits all wavelengths of the spectral domain to generate images. Such methodologies have undergone significant developments in recent years and will be detailed in section 4.

2.4 Quantification

In LIBS-based imaging analysis, the term “quantification” is not truly appropriate, since the measurement is performed in a single-shot configuration, and there are, therefore, no statistics related to the intensity associated with a single pixel of an image. However, several works have reported “semiquantitative” imaging using various types of matrices. The most common calibration method uses reference materials with known concentrations and compositions similar to those of the sample of interest to be analyzed under similar conditions to build calibration models. For example, the quantitative imaging of steel⁶⁰, boron-doped crystalline silicon⁶¹, glass^{52,53}, and biological and other materials^{62–64} has already been reported. When reference materials are unavailable, one possibility is to regard the imaging dataset as representative of the entire sample volume. The global elemental

composition is then retrieved afterward using complementary analytical approaches, such as XRF or ICP-based analysis, and then used to calibrate the imaging experiments in a semiquantitative approach. Several examples of using this strategy, such as those involving Ti-doped sapphire⁶⁵, lithium ore²⁹, copper-nickel ore³¹, murine kidney⁶⁶, or heterogeneous catalysts⁶⁷, have been reported. In other cases, additional imaging techniques may be applied to calibrate the LIBS measurements. Trichard et al. used a profile measurement performed with an electron microprobe (EPMA) of palladium (Pd) on a catalyst section⁶⁷. In this work, several lines of Pd with various intensities were exploited to cover the entire concentration range without being affected by self-absorption. An equivalent methodology was used for the characterization of piezoelectric crystals⁶⁸. More recently, the use of EPMA to calibrate both μ LIBS and μ XRF images was proposed by Fabre et al. to obtain mineralogical maps of the studied geological samples. In addition, Cugerone et al. used LA-ICP-MS analysis to study different positions of samples to calibrate LIBS measurements and quantify the germanium (Ge) in Pb-Zn ore deposits^{69,70}.

3. Promising applications

LIBS, in general, has almost limitless applications, but in some cases, qualitative and/or quantitative measurement is not enough, and spatial information is needed. In this section, we highlight a limited number of recent and high-quality research studies that align with the most promising application fields, keeping in mind that the selected articles demonstrate the interest and added value of using LIBS imaging compared to more conventional LIBS bulk analysis.

3.1 Industry

The capabilities of LIBS make it uniquely advantageous for industrial applications. The implementation of LIBS in industry started several decades ago and was facilitated by a few researchers. Among them, Reinhard Noll initiated the development of LIBS applications for steel analysis in 1995⁷¹. He recently reported the use of a full-imaging LIBS system for end-of-life industrial products⁷². The system offers 2D and 3D imaging (from both camera and LIBS) and can localize elements of interest (such as Ta and Cu) within industrial products for

their recycling. In addition to this example, we will present some industrial fields in which LIBS imaging has been applied.

3.1.1 Material analysis for manufacturing applications

This section presents several applications related to material analysis, covering a wide range of industrial applications in which LIBS imaging can have a greater impact than single-shot LIBS. For example, Lee et al. used LIBS imaging to monitor the processing of solar cells⁷³. Small maps were generated (20x20 pixels) with a resolution of 130 μm with a top-hat laser beam for tracking the spatial composition of Se, Cu, Ga and In. The LIBS signal was also correlated with secondary ion mass spectrometry (SIMS). Sdvizhenskii et al. conducted an analysis of the quality and uniformity of laser cladding coatings⁷⁴. The authors used LIBS imaging because an energy dispersive X-ray (EDX) experiment failed to measure carbon. With a spatial resolution of 40 μm , they were able to produce 3D elemental maps, with 38% of the laser spot overlapping for ablating a line and avoiding the effects of crater formation. Weiss et al. imaged fluorine with LIBS⁷⁵. Since fluorine is difficult to detect, they opted for detecting the molecular emission of both CaF and CuF. Using a copper coating on top of the sample, the LoDs for CaF and CuF were 160 and 240 ppm, respectively. Moreover, they had to increase the laser energy by a factor of 4 (from 1.6 mJ to 6.5 mJ per pulse) to obtain the same LoD with the atomic F line at 685.6 nm. This improvement can be useful in the lime industry, in which keeping an eye on chlorine (Cl) and F concentrations is necessary. Agresti et al. already used LIBS imaging with a handheld (HH) LIBS system for quality control in calcareous rock for the lime industry⁷⁶. Elemental mapping was used as a support for controlling the homogeneity of the rocks, and accumulated single-shots were used on a PLS- and ANN-based model for compositional prediction.

LIBS imaging was also employed to investigate the homogeneity of lead-free piezoelectric crystal growth⁶⁸. Maps of Ca and Zn were produced at a resolution of 12 μm , and the intensities were calibrated by EPMA. Transversal analysis of the crystal fibers

showed Ca and Zn inhomogeneity, which can lead to different electrical or mechanical properties. Similar research on crystal growth has shown the segregation of Al, Sr and Ca impurities⁷⁷. Park et al. generated LIBS images of lithium-ion batteries (LIBs) after different laser structuring, which can increase battery capacity⁷⁸. The lithium elemental distribution of battery electrodes, which were 140x200 μm in size, was shown at a resolution of 12 μm (Figure 3a). The corresponding elemental maps exhibited different lithium distributions for each pattern induced by the laser and an increase in the interfacial surface area between electrodes of up to 260%. Finally, Grünberger et al. proposed an innovative LIBS-based imaging system for analyzing polymers⁷⁹. The laser pulse energy was drastically decreased to only produce seed electrons at the sample surface, which triggered a spark that excited the smaller ablated material. LIBS offered better sensitivity for neutral lines and molecular emission, but laser ablation-spark discharge-optical emission spectroscopy (LA-SD-OES) produced a higher ionic signal while decreasing the laser energy.

3.1.2 Oil industry and corresponding catalysts

From the extraction process to the final sale, oil undergoes successive refining steps. Some of them include the use of aluminum-based catalysts. It is thus of prime importance to control those catalysts during the process to ensure the refining quality. Indeed, after a certain time in the oil, catalysts may be deactivated due to external contamination, mainly from carbon. To quantify this impregnation, the selected technique should cover a large dynamic range of carbon concentrations, from ppm to tens of %mass, which perfectly aligns with the LIBS capabilities. In a recent study, Jolivet et al. monitored the carbon concentration in freshly impregnated catalysts at different times, from 30 min to 6 weeks⁸⁰. Quantitative LIBS imaging was performed with a resolution of 25 μm to observe the dynamics of C absorption inside the catalysts, with an LoD of 305 ppm. In another study, Trichard et al. used the same setup and produced quantified images of trace metal impurities in the same kind of catalysts for V, Ni and S in addition to C⁸¹, as shown in Figure 3b. Finally, the same group monitored catalyst maturation processes to understand and optimize their activation kinetics⁸².

3.1.3 Nuclear applications

Following the general movement toward green energy production, the nuclear industry is currently pushing the development of new generation fission cores and the first fusion core prototypes. In the latter case, the core environment is drastically different from the fission one: hot plasma has to be maintained to produce energy. This plasma can corrupt the surrounding walls inside the core by corrosion and/or erosion. Thus, there is a need for a technique that can remotely characterize the integrity of these walls. LIBS showed great promise for this specific application with an adapted setup and protocol. For example, the wall surface can be regarded as some number of square meters, so the resolution should be lower for meaningful sampling. In addition, picosecond lasers can be used to control the ablation rate at the lowest value possible. Two articles were published using these specific setups. In the first one, elemental and quantified erosion images were produced with a spatial resolution of 5 mm from typical graphite tiles used in reactors after being exposed to He/H plasma⁸³. These 2D images corresponded to one direction and depth analysis. 200 shots were produced for the depth, resulting in images in the range of 0 to 350 mm in the poloidal coordinates and down to several μm in depth. The second article used the same experimental conditions, except that the authors produced a 3D image by adding a toroidal component and thus were able to quantify the erosion degree in a 3D map with dimensions of 7 cm x 5 cm x 4 μm ⁸⁴ (Figure 3c). Finally, Choi et al. detected radioactive hotspots in nuclear power plants by conducting an isotopic analysis of iron in structural material from the nuclear core⁸⁵. By using double-pulse LIBS with a 355 nm wavelength for ablation and 1064 nm for reheating, the authors were able to distinguish ^{54}FeO molecular emission from ^{56}FeO molecular emission and even produced an isotopic map with a resolution of 500 μm , showing the potential for double-pulse LIBS imaging for nuclear materials.

3.1.4 Pharmaceutical industry

Despite being a robust analytical tool, LIBS imaging is rarely used for pharmaceutical studies. Pharmaceutical companies have to test the efficiency and purity of drugs. In addition, public health organizations can provide analysis on drugs or for hazardous element detection. In this regard, Zou et al. performed 3D elemental imaging on drug tablet coatings with a resolution of 50 μm ⁸⁶. The image depth was produced by using 30 pulses at each location on the map. In this work, the authors characterized the thickness and uniformity of

tablet coatings, which play key roles in drug kinetics. The same team conducted LIBS imaging on an injectable implant for monitoring drug release by looking at the fluorine (F) line at 685.6 nm⁸⁷. With a lateral resolution of 35 μm , they were able to track implant life-duration as illustrated in Figure 3d.

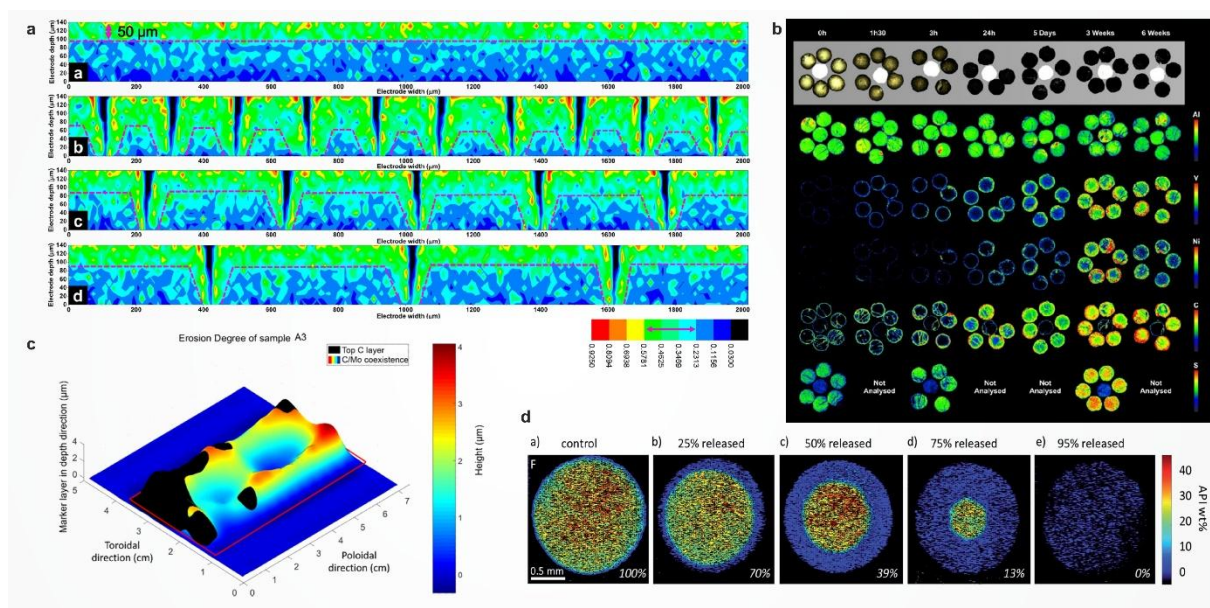


Figure 3: Industrial applications of LIBS imaging.

a) Elemental map of Li from LIBs after different laser patterning. Reprinted from Journal of Energy Chemistry, Vol 64, J. Park, H. Song, I. Jang, J. Lee, J. Um, S. Bae, J. Kim, S. Jeong, H-J. Kim, Three-dimensionalization via control of laser-structuring parameters for high energy and high power lithium-ion battery under various operating conditions, pp. 93-102. Copyright (2022), with permission from Elsevier. (ref ⁷⁸)

b) Al, V, Ni, C and S maps from catalysts. Reprinted from Applied Surface Science, Vol 532, R. Yi, D. Zhao, J. Oelmann, S. Brezinsek, M. Rasinski, M. Mayer, C. Prakash Dhard, D. Naujoks, L. Liu, J. Qu, 3-Dimensional analysis of layer structured samples with high depth resolution using picosecond laser-induced breakdown spectroscopy, p. 147185. Copyright (2020), with permission from Elsevier. (ref ⁸¹)

c) Quantitative 3D erosion map from graphite tiles after exposure to He/H plasma. Reprinted from Journal of Catalysis, Vol 363, F. Trichard, F. Gaulier, J. Barbier, D. Espinat, B. Guichard, C-P. Lienemann, L. Sorbier, P. Levitz, V. Motto-Ros, Imaging of alumina supports by

laser-induced breakdown spectroscopy: A new tool to understand the diffusion of trace metal impurities, pp. 183-190. Copyright (2018), with permission from Elsevier. (ref ⁸⁴)

d) Drug implant decay after different in vitro times monitored through F elemental maps. Reproduced from L. Zou, M. J. Stenslik, M. B. Giles, J. Ormes, M. Marsales, C. Santos, B. Kassim, J. P. Smith, J. J. Gonzalez, X. Bu. Journal of analytical atomic spectroscopy 1986, 34, 1351-1354 (ref ⁸⁷), with permission from The Royal Society of Chemistry.

3.2 Geology

In recent years, geologists and geochemists have shown increasing interest in LIBS imaging. Compared to those of the usual techniques, either the sensitivity, resolution and/or speed of analysis were improved^{24,88-90}. In this section, trending applications of LIBS imaging for geological sample characterization are presented.

3.2.1 Paleo-climate

Speleothems and ice cores are paleo-climate archives. Paleo-temperature is able to be studied either by analyzing the oxygen isotopic ratios of ice cores⁹¹ or some elemental ratios of speleothems⁹². In the latter case, LIBS images were produced directly on site²³ and in the laboratory^{7,34}. The corresponding micrometric lateral resolution, down to 10 μm , allows distinguishing speleothem laminae growth, leading to the possible determination of biennial temperatures for large eras (Figure 4a). The same type of information was also obtained by analyzing marine mollusk shells, with a resolution of 100 μm ⁹³.

3.2.2 Strategic elements

To achieve the Climate Neutrality Objectives, several countries and supra-national entities (such as the European Union) aim to reduce the transport sector's contribution to greenhouse gas emissions. In particular, moving toward zero-emission vehicles will be a crucial point of this strategy. To achieve this transition, a sufficient amount of lithium must be extracted to produce enough batteries, and lithium production is expected to grow by a factor of 5 in less than 10 years according to the World Economic Forum (WEF). Thus, there is a crucial need for a technique capable of identifying lithium in ore or directly at the mining site. Recently, we have witnessed an improvement in LIBS imaging both in laboratories and

directly on-site with handheld instruments, which can be regarded as the two processes of mine settlement. First, different locations are prospected, and mineral cores are extracted and sent to laboratories for analysis. Preconstructed setups can provide sensitive results in the range of ppm, with a resolution ranging from 40 to 200 μm according to the core size, at a high speed of analysis²⁹. The major strengths of such setups from EMISSION are the speed of analysis and the ability to conduct scanning directly on the drill core. In complement, additional strategic elements can be detected almost automatically by using semisupervised algorithms^{94,95}.

Once the location of the mining site has been determined from the laboratory analysis, portable LIBS instruments can be used directly on site to guide the mining expansion^{96,97}. Even though the sensitivity and resolution of such handheld instruments are limited, they provide fast results that can strongly affect mining extraction efficiency. Indeed, lithium is not the only critical, strategic or precious element. As an example, LIBS imaging has been used to produce 3D images of gold ore with a kHz frequency rate, resulting in an $8 \times 6 \times 1 \text{ mm}^3$ map obtained in 20 min of analysis⁹⁸. LIBS imaging can also identify gold veins in ore at kHz speed³⁰, quantify hydrocarbons in petroleum-rich samples⁹⁹, or even detect and identify Pt and Pd in ore extremely quickly¹⁰⁰, leading to a more efficient mining extraction process. In addition, several applications and industries require rare earth elements (REEs) or rare metals. Such elements can be challenging to detect in the ppm range, even if, in some cases, LIBS alone can detect the elements of interest. In a study from Fabre et al., megapixel elemental maps with a spatial resolution of 15 μm of more than 20 elements were produced, most with a sensitivity close to the ppm level¹⁰¹.

In another study, Baele et al. successfully correlated EDS quantitative measurements with LIBS imaging signals for 8 elements, including As and Sb¹⁰², as shown in Figure 4b. However, quantification appears challenging when no standards are available, as external methods may not be sensitive enough for some elements. Some methods have been proposed by combining LIBS imaging and innovative data processing to achieve an accurate phase distinction inside a mineral sample to efficiently identify and quantify elements of interest. As an example, k-mean clustering has been successfully applied, combined with spatial raster analysis, for the detection of La¹⁰³. Another way to solve this issue is to combine several detection approaches. An easy method might be to adjust the temporal

acquisition of the signal for detecting molecular emission or plasma-induced luminescence (PIL). In this regard, the combination of typical LIBS imaging for atomic and molecular emission, as well as luminescence, allowed easy imaging of elements such as Eu, Gd or Sm¹⁰⁴, with extremely competitive LoDs of 10, 40 and 40 ppm, respectively. Finally, we present the possibilities offered by combining two different but complementary techniques: LA-ICP-MS and LIBS imaging of uranium ore¹⁰⁵. Briefly, LIBS was used to perform a rough and rapid scan to map the total area. Then, LA-ICP-MS was used in specific and restricted areas where U was detected. LA-ICP-MS is typically more sensitive than LIBS and provides isotopic information; however, it is only used for imaging smaller regions.

3.2.3 Fundamental applications

Aside from specific geological applications, LIBS imaging can also offer solutions to more fundamental issues. Several minerals produce very complex and heterogeneous samples, and phase discrimination and classification can be challenging because different phases can have the same elemental compositions but at different concentration ratios. Zivkovic et al. used an unsupervised clustering algorithm combined with CF-LIBS for an accurate classification of the different phases in an archaeological mortar¹⁰⁶. In another study from Cugerone et al., a combination of LA-ICP-MS, electron backscattered diffraction (EBSD) and LIBS imaging was employed for sphalerites, a typical rock mineral that contains rare metals (Ge, Ga, In, Cd)⁷⁰. By combining all the information from the different techniques, the elemental behavior and distributions were correlated with the geographical location of the minerals, which may provide significant insight into how the rock is formed. The same group of authors had already conducted a prospective work on this topic by studying the Ge distribution of sphalerite with coupled LIBS imaging and EBSD⁶⁹. On the other hand, from a totally different perspective, Nardecchia et al. combined PIL and LIBS imaging to study a kyanite crystal¹⁰⁷ (Figure 4c). The PIL signal in imaging mode can be complex, and due to its long emission, two successive signals might overlap. The aim of this work was to use LIBS imaging data to scale PIL data by compressing and fusing both data, opening the way for fusing data between LIBS and other techniques.

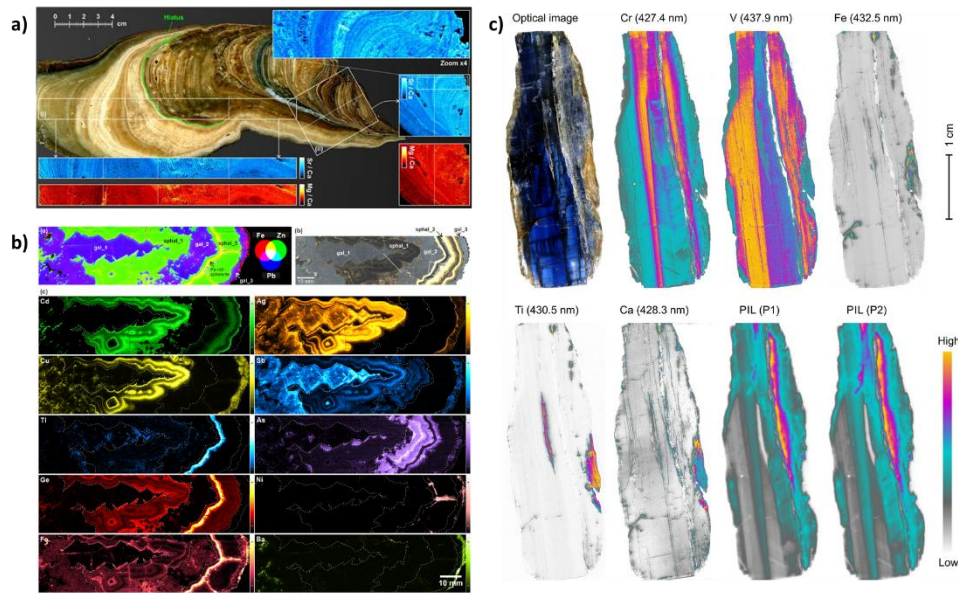


Figure 4: Geological applications of LIBS imaging.

a) Speleothem imaging of the Sr/Ca ratio (blue) and Mg/Ca ratio (red). Reprinted by permission from Macmillan Publishers Ltd: *Scientific Reports* 2017, 7, 5080, Cáceres, J. O.; Pelascini, F.; Motto-Ros, V.; Moncayo, S.; Trichard, F.; Panczer, G.; Marín-Roldán, A.; Cruz, J. A.; Coronado, I.; Martín-Chivelet, J. Megapixel Multi-Elemental Imaging by Laser-Induced Breakdown Spectroscopy, a Technology with Considerable Potential for Paleoclimate Studies (ref⁷), copyright (2017)

b) Various elemental maps from different elements of Zn-Pb ore. Reprinted with permission from *Geol. Belg.* **2021**, 24, 125–136, Baele, J.-M.; Bouzahzah, H.; Papier, S.; Decrée, S.; Verheyden, S.; Burlet, C.; Pirard, E.; Franceschi, G.; Dejonghe, L. Trace-Element Imaging at Macroscopic Scale in a Belgian Sphalerite-Galena Ore Using Laser-Induced Breakdown Spectroscopy (LIBS). (ref¹⁰²)

c) Elemental and plasma-induced luminescence maps from a blue kyanite crystal. Reprinted from *Analytica Chimica Acta*, Vol 1192, A. Nardecchia, A. de Juan, V. Motto-Ros, M. Gaft, L. Duponchel, Data fusion of LIBS and PIL hyperspectral imaging: Understanding the luminescence phenomenon of a complex mineral sample, p. 339368. Copyright (2021), with permission from Elsevier. (ref¹⁰⁷)

3.3 Forensic application

Due to its fast use and sensitivity in the ppm range for most elements, LIBS is already employed in forensic applications, such as determining gunshot residues (GSR)¹⁰⁸ or in various other forensic situations in its single-shot modality¹⁰⁹. LIBS imaging is currently being evaluated for the same GSR analysis as well as for shooting distance determination⁵⁴. In both studies from Vander Pyl et al. and Lopez et al., LIBS imaging was applied to targets after shooting from different distances^{54,110}. By looking at the Ba and Pb elemental distributions, the authors demonstrated that the elemental pattern distribution depends on the shooting distance, and it may be possible to estimate the shooting distance from LIBS imaging. With the rapid development and affordability of LIBS imaging setups, new applications related to the forensic field are starting to appear. These “exotic” applications show promising results, which might cause forensic applications of LIBS imaging to increase in the future. Rather than a complete review in this field, which is available elsewhere¹¹¹, we will present a subjective selection of research articles in which LIBS imaging was demonstrated to hold great promise for forensic studies.

Yang et al. were able to differentiate fingerprints from two different people using single-shot LIBS and principal component analysis (PCA)¹¹². LIBS imaging was employed with a lateral resolution of 125 μm to reconstruct each fingerprint in an overlap situation, as illustrated in Figure 5a. The same research group published a similar work, in which the aging effect was also considered using soft independent modeling of class analogy (SIMCA)¹¹³. This breakthrough might be useful in crime investigation when fingerprints need to be analyzed: in this specific case, rapid LIBS imaging analysis can identify fingerprint authors and even deconvolute multiple overlapping fingerprints due to the specific chemical composition of each individual fingerprint. Moreover, Hilario et al. used LIBS imaging for handwritten documents¹¹⁴. By using PCA maps, two inks of the same color were tested to identify any “fake” written information added to a document (Figure 5b). Even if the difference between the writing of two pens was not visible to the naked eye, LIBS imaging produced two different PCA scores for each ink, leading to their identification. This promising application can be useful to prove the veracity of official handwritten documents. LIBS imaging was also used for steganography¹¹⁵: by using inks with different elemental compositions, Yin et al. were able to reveal hidden messages in a handwritten document, as shown in Figure 5c.

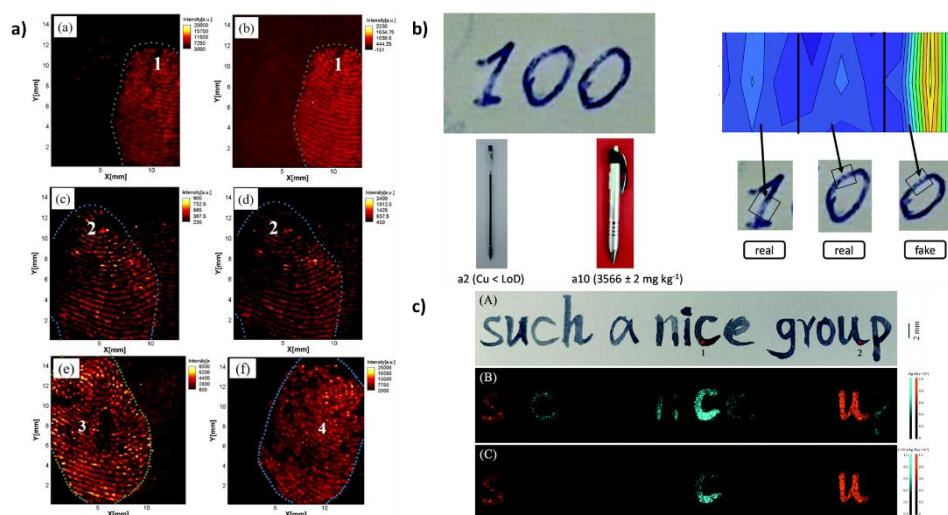


Figure 5: Forensic applications of LIBS imaging.

a) Elemental images of overlapping fingerprints for different elements. Reprinted from *Spectrochimica Acta Part B: Atomic Spectroscopy*, Vol 134, J-H. Yang, S-J. Choi, J. J. Yoh, Toward reconstruction of overlapping fingerprints using plasma spectroscopy, pp. 25-32. Copyright (2017), with permission from Elsevier. (ref ¹¹²)

b) PCA maps based on LIBS imaging highlighting which number was added. Reproduced from Ferri Hilario F, Lime de Mello M, Edenir R. *Analytical Methods: ad. Meth appl.* 2009, 13, 232-241 (ref ¹¹⁴), with permission from The Royal Society of Chemistry.

c) Elemental images of handwritten documents using different inks. Reproduced from P. Yin, E. Yang, Y. Chen, Z. Peng, D. Li, Y. Duanb, Q. Lin. *Chemical Communications* 2021, 57, 7312-7315 (ref ¹¹⁵), with permission from The Royal Society of Chemistry.

3.4 Biology and medicine

The direct imaging of endogenous chemical elements in plants or in animal and human tissues is of paramount interest for a global description of the pathophysiological state of organs.

LIBS microscopy can be used to monitor the elemental composition of any kind of sample. In regard to studying biological or biomedical specimens, the ability to interpret 2D elemental

images of chemical elements with LIBS imaging provides more information compared to the single-shot microanalysis strategy performed with LIBS or competitive technology. In fact, elemental imaging with LIBS provides researchers and clinicians with the possibility of collecting the complete spectrochemical information of the entire surface of the specimen of interest, without bias or *a priori*. This point is particularly important because biomedical specimens are highly heterogeneous in terms of cellular content. Each organism is composed of several tissues, and each tissue is made of several cell types. The cell diversity in vegetal, animal and human tissues is incredible, as is pathophysiological cellular chemical content. As an example, in a given tissue area of a few hundred square micrometers, one can find bone tissue next to muscular cells, with surrounding epithelial cells and neighboring blood vessels containing blood cells. Except for the analysis of blood or other body fluids, the advantage of tissue elemental imaging over single-shot microanalysis is obvious in biomedicine, and we strongly encourage the LIBS community to embrace this strategy for analyzing biomedical tissues with LIBS. A few reviews have already described the relevance of LIBS imaging for biomedicine³⁻⁵; however, in this section, we will focus on more recent applications of label-free LIBS elemental imaging for biology and medicine, discussing how this tool is facilitating a broader understanding of the role of metals in systems biology and how environmental exposure can be monitored in plant, animal and human pathology.

The French research group of Dr Motto-Ros historically took the initiative in the development and improvement of the LIBS technique for bioimaging the elemental content of animal organs¹⁹. A cornerstone study reported the ability to use ultraviolet-based LIBS imaging to study the distribution of gadolinium-silicon-based nanoparticles in a multielemental and quantitative manner⁶. The elemental analysis was performed in murine epoxy-embedded kidneys collected at different timepoints after intravenous injections (Figure 6a), and an image resolution of 40 μm was achieved.

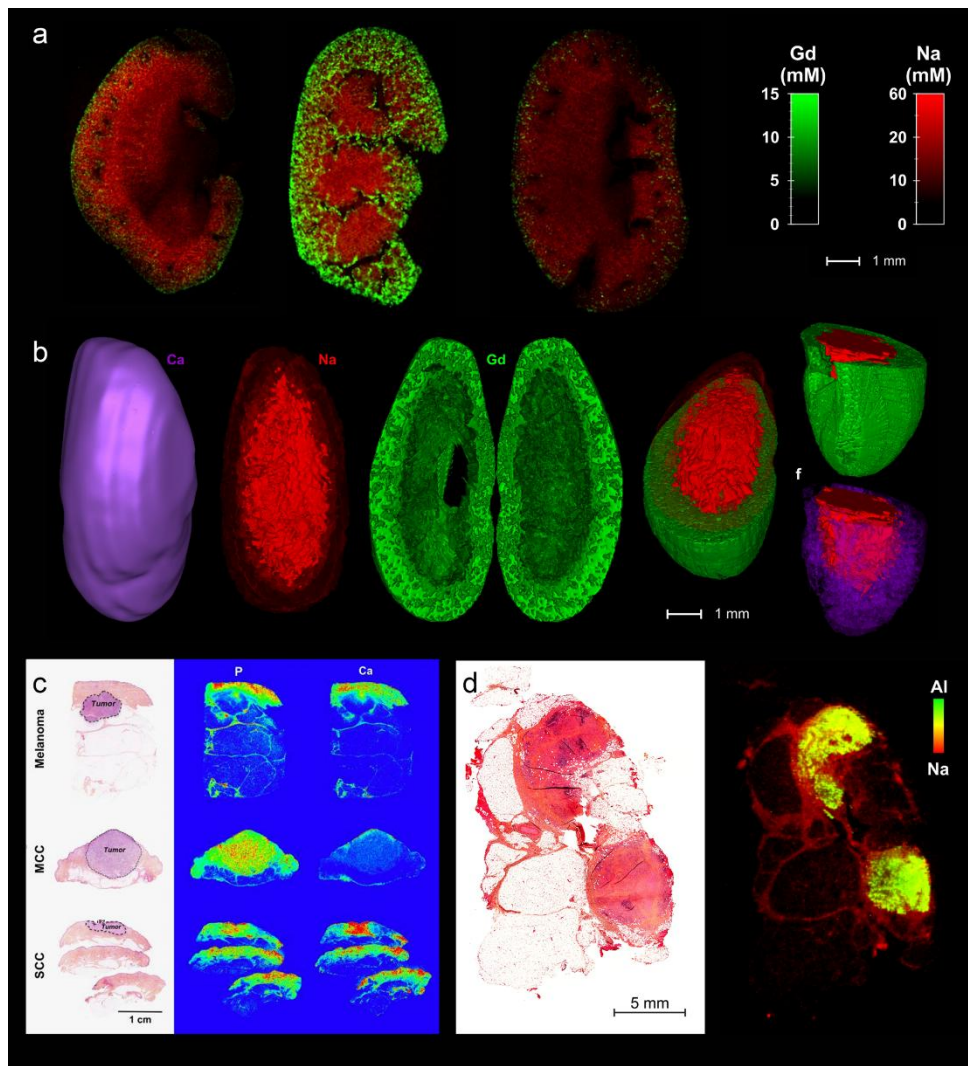


Figure 6: Historical milestones in LIBS imaging for biomedical applications

(a) Distribution of gadolinium-based nanoparticles in the kidney as a function of the time elapsed postadministration. Quantitative imaging of Gd (green) and Na (red) in coronal kidney sections. The images were recorded at a 40 μm resolution and represent 30,000 pixels. Reprinted by permission from Macmillan Publishers Ltd: Scientific Reports, Laser spectrometry for multi-elemental imaging of biological tissues. Sancey, L.; Motto-Ros, V.; Busser, B.; Kotb, S.; Benoit, J. M.; Piednoir, A.; Lux, F.; Tillement, O.; Panczer, G.; Yu, J. Sci Rep 2014, 4, 6065 (reference citation ⁶), copyright (2014).

(b) 3D imaging at the whole-kidney scale; Ca (violet), Na (red), and Gd (green) are shown. Right part: Kidney sections allowing the observation Gd and Na combined on coronal or axial sections or with Ca. Reprinted by permission from Macmillan Publishers Ltd: Scientific Reports, 3D Imaging of Nanoparticle Distribution in Biological Tissue by Laser-Induced Breakdown Spectroscopy. Gimenez, Y.; Busser, B.; Trichard, F.; Kulesza, A.; Laurent, J. M.;

Zaun, V.; Lux, F.; Benoit, J. M.; Panczer, G.; Dugourd, P.; Tillement, O.; Pelascini, F.; Sancey, L.; Motto-Ros, V. *Sci Rep* 2016, 6, 29936 (reference citation ⁶⁶), copyright (2016).

(c) Elemental imaging of different skin cancer types. Left panel: histological image of the three studied skin cancer types after hematoxylin-eosin-saffron (HES) staining (melanoma metastasis, Merkel cell carcinoma (MCC) and squamous cell carcinoma (SCC)). The different skin layers, i.e., the epidermis, dermis, and hypodermis, are visible, and the dashed line indicates the tumor region. Right panel: P and Ca elemental distributions shown with a cold-to-warm color scale. Reprinted from *Spectrochimica Acta Part B: Atomic Spectroscopy*, Vol 133, Moncayo S., Trichard F., Busser B., Sabatier-Vincent M., Pelascini F., Pinel N., Templier I., Charles J., Sancey L. Motto-Ros V., *Multielemental imaging of paraffin-embedded human samples by laser-induced breakdown spectroscopy*, pp. 40-44. Copyright (2017), with permission from Elsevier. (ref ¹¹⁶)

(d) Histopathological morphology of a cutaneous granuloma with corresponding elemental images obtained after LIBS (right panels). LIBS analysis revealed high levels of aluminum (Al, in green) in the immunohistiocytic areas. Sodium (Na, in red) enabled the visualization of the global tissue architecture. Reprinted by permission from Macmillan Publishers Ltd: *Modern Pathology, Characterization of foreign materials in paraffin-embedded pathological specimens using in situ multi-elemental imaging with laser spectroscopy*. Busser, B.; Moncayo, S.; Trichard, F.; Bonneterre, V.; Pinel, N.; Pelascini, F.; Dugourd, P.; Coll, J. L.; D'Incan, M.; Charles, J.; Motto-Ros, V.; Sancey, L. *Mod Pathol* 2018, 31, 378–384 (reference citation ¹¹⁷), copyright (2017).

The same team subsequently switched to an infrared laser source to image in 3D the same small theranostic nanocompounds in kidneys and at the whole-organ scale (Figure 6b). They successfully managed to improve the accessible resolution as low as $\sim 10 \mu\text{m}$ in all 3 dimensions⁶⁶. They logically further developed their expertise to focus on the imaging of human specimens. They obtained the proof-of-concept for mastering the ablation process for the 2D-LIBS multielemental analysis of soft matrices, i.e., human paraffin-embedded skin biopsies, generating descriptive multielemental maps of the endogenous elements distributed within normal skin and a series of skin cancers (Figure 6c)¹¹⁶. Interest in the use of LIBS imaging for medicine was first demonstrated by analyzing the elemental content of abnormal histopathological features, such as pigments or vacuoles, reported in human

granulomas, lymph nodes, or scar specimens. LIBS imaging provided evidence of exogenous soluble compounds, such as aluminum salts (Figure 6d), micro- or nanosized metal particles made of titanium or tungsten and even pure copper foreign bodies¹¹⁷.

3.4.1 Elemental imaging of plants

For plants, LIBS imaging can be performed on different parts, such as the root, stem, flower or fruit.

The collected information is useful for understanding potential nutrient dysregulations (Na, K, P...) that reflect general plant health as well as diseases, insufficient nutritional intake, and even possible contamination by polluted atmosphere, water, and/or soils¹¹⁸.

With the aim of investigating the spatial control of nutrient exchange in plant rhizospheres, LIBS elemental imaging was used to image both organic content and inorganic constituents in root-rhizosphere-soil systems¹¹⁹. This study included the generation of elemental images for 17 macronutrients, micronutrients, and matrix elements from soil, with a resolution of ~100 µm. One of the main results was the observation of fine-scale chemical gradients within small samples of ~1 mm of switchgrass roots. This demonstrated that LIBS imaging is suitable as an effective spatially resolved technique for the sensitive and rapid elemental mapping of complex soil matrices and plant rhizospheres, with simultaneous multielement acquisition and minimal sample preparation or destruction.

LIBS elemental bioimaging was also used to measure the effects of selenium enrichment on the distribution of diffusible endogenous cations in edible *Pleurotus* mushrooms¹²⁰. This study led to the conclusion that selenium enrichment altered the distribution of K and Mg and increased Ca bioaccumulation in the lower part of the pink oyster mushroom (*Pleurotus djamor*). From these results, it was deduced that selenium altered Ca, K and Mg transport and compartmentalization, thus impacting global fungal metabolism.

Because of its ability to analyze lightweight elements, LIBS imaging was advantageously chosen to analyze the presence of lithium in the leaves of *Podocarpus macorophyllus*¹²¹. Similarly, a double-pulse strategy was employed to study the chromium distribution in rice leaves¹²².

In an attempt to improve the sensitivity and ability of detecting harmful chemicals in plants, a recent study employed a strategy based on the use of nanoparticle-enhanced laser-

induced breakdown spectroscopy (NELIBS), a technique invented by the group of Prof. De Giacomo¹²³.

The distribution of toxic agents, such as chlorpyrifos and cadmium, was analyzed in the leaves and stems of lettuce in a space-resolved manner. The main findings were that heavy metals are distributed unevenly in edible plant leaves, with higher concentrations in veins than in mesophyll. In this study, NELIBS achieved an increased sensitivity by two orders of magnitude compared to the standard LIBS technique¹²⁴.

Recently, LIBS imaging was used to help describe the cadmium distribution in the white mustard crop plant (*Sinapis alba* L.)¹²⁵. The authors used a combination of LIBS imaging and micro-LIBS to achieve lateral resolutions of 100 μm and 25 μm , respectively. This allowed to observe the spatial cadmium distribution in plant roots exposed to either CdCl_2 solutions or cadmium telluride quantum dots (CdTe QDs, Figure 7).

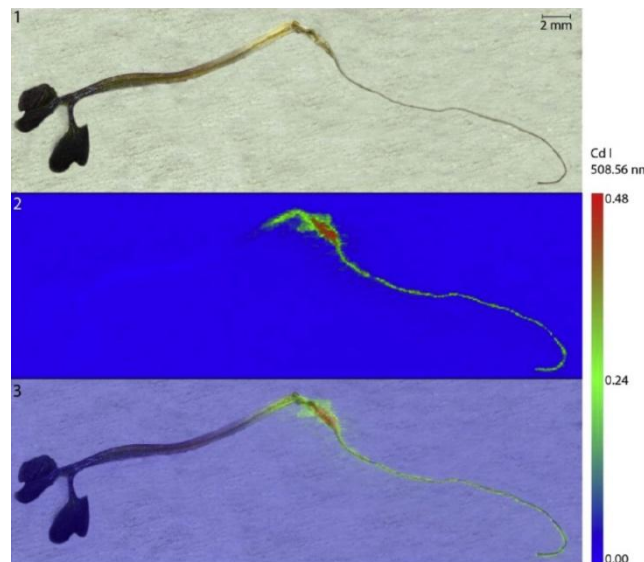


Figure 7: Example of LIBS elemental images of plants. 1. Photograph of *Sinapis alba* plants exposed to CdTe QDs before LIBS measurements. 2. LIBS elemental map constructed for the Cd I 508.56 nm emission line (spatial resolution of 100 μm). 3. Overlap of the original photograph of a plant with a LIBS map. The scale shows the total emissivity of the selected emission line. Reprinted from Chemosphere, Vol 251, P. Modlitbová, P. Pořízka, S. Střítežská, Š. Zzulka, M. Kummerová, K. Novotný, J. Kaiser, Detail investigation of toxicity, bioaccumulation, and translocation of Cd-based quantum dots and Cd salt in white mustard, pp. 126174. Copyright (2020), with permission from Elsevier. (ref ¹²⁵)

3.4.2 Elemental imaging of animal tissue

LIBS imaging has been used in a wide range of applications for analyzing animal tissues. Notably, it appears that this technique is well suited for imaging the pharmacokinetics of metal-based nanoparticles and therapeutics in the organs of animals or the pathophysiological state of endogenous elements in tissues.

LIBS was notably used for imaging the distribution of ultrasmall luminescent gold (Au) particles referred to as nanoclusters (NCs)¹²⁶. In combination with X-ray fluorescence, LIBS imaging allowed the proper visualization of Au in the organs and the tumors of animals that were previously injected with Au NCs. This work is of importance since it demonstrated once again that LIBS is an easy and inexpensive method for evaluating the pharmacokinetics of metal-NPs in organisms. Here, LIBS determined a high accumulation of Au in the kidney (Figure 8a), whereas Au was barely detected in the liver and spleen. From this, it was obvious that these innovative compounds were preferentially eliminated through the urine on a very fast timescale. In complement, LIBS effectively measured the accumulation of Au-based nanocompounds in tumors that were subcutaneously grafted. This work also underlines the benefit of combining tissue-scale elemental imaging, such as LIBS, with subcellular-scale elemental imaging modalities, such as X-ray fluorescence, for collecting complementary information.

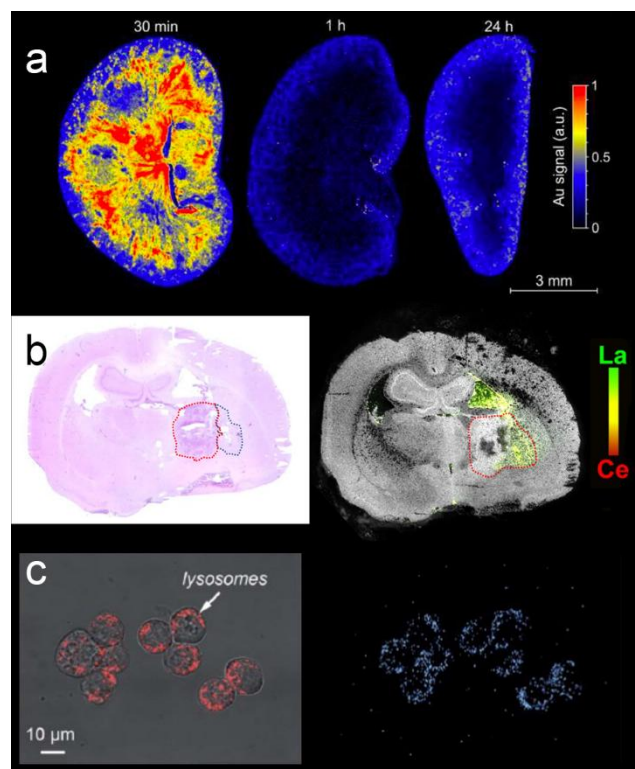


Figure 8: LIBS imaging in biological applications for animal tissues and cells.

(a) Kidney slice images obtained 30 min, 1 h, and 24 h postinjection of Au NPs. Reproduced from Elemental and optical imaging evaluation of zwitterionic gold nanoclusters in glioblastoma mouse models. X. Le Guével, M. Henry, V. Motto-Ros, E. Longo, M. I. Montañez, F. Pelascini, O. de La Rochefoucauld, P. Zeitoun, J-L. Coll, V. Josserand, L. Sancey. *Nanoscale* 2018, 10, 18657-64 (ref ¹²⁶), with permission from The Royal Society of Chemistry.

(b) Brain section with a glioma, surrounded by the red dashed line, several days after the local administration of LaCe NPs (DOI 10.1016/j.jneumeth.2022.109676). Reprinted from *Journal of Neuroscience Methods*, Vol 379, B. Busser, A-L. Bulin, V. Gardette, H. Elleaume, F. Pelascini, A. Bouron, V. Motto-Ros, L. Sancey, Visualizing the cerebral distribution of chemical elements: A challenge met with LIBS elemental imaging, pp. 109676. Copyright (2022), with permission from Elsevier. (ref ¹²⁷)

(c) Nanoscale LIBS imaging of InP nanoparticles within single cells. Optical image of cells stained with LysoTracker Red DND-99 (left) and LIBS imaging of In(I) at 410.2 nm (right). Reproduced from *Nanoscale laser-induced breakdown spectroscopy imaging reveals chemical distribution with subcellular resolution*. Y. Meng, C. Gao, Z. Lin, W. Hang, B. Huang. *Nanoscale Advances* 2020, 2, 3983 (ref ¹²⁸), with permission from The Royal Society of Chemistry.

It has been established that the choice of instrumental analytical technique is crucial for imaging metal-nanocompounds in tissues¹²⁹. In the specialized field of brain elemental imaging, almost all elemental imaging modalities have been employed for the direct imaging of diffusible ions, such as Na⁺, Mg²⁺, Ca²⁺, K⁺, and Cl⁻, within brain tissue¹³⁰. In this aforementioned article, the global landscape of techniques described for brain elemental imaging included proton-induced X-ray emission (PIXE), X-ray fluorescence microscopy (XFM), SIMS, and laser-ablation inductively coupled plasma–mass spectrometry (LA-ICP–MS). However, LIBS imaging was not included in the list despite being a method of choice for imaging brain tissues. Yet, LIBS may be very effective and helpful for researchers specializing in both nanomedicine and neurology¹²⁷. The visualization of endogenous chemical elements, such as P, Mg, Ca, Na, Cu and Fe, was easily achieved with LIBS. The corresponding chemical maps described the localization of these elements of interest in animal brain cryosections obtained from adults and even from mouse embryos. The ability

to image and quantify zinc in the fetal brain with LIBS allowed us to study the distribution and time-course regulation of zinc during the development and maturation of cerebral structures during embryogenesis. What was shown for zinc remains true for any other endogenous chemical element, and LIBS should become one of the most reliable and user-friendly methods for evaluating the spatial and temporal regulation of metal homeostasis at the whole-organ scale. In a different study, LIBS was also used to image Ca, Mg, Na, Cu, and P distributions in 10 mouse brain sections¹³¹. Here, again, LIBS demonstrated its capacity to image at the whole-organ scale, with the ability to perform 3D imaging.

Bulin et al. also used LIBS imaging as a key analytical modality to image lanthanide-cerium-based nanoscintillators¹³². These LaF₃:Ce nanocompounds were imaged in rat brains bearing orthotopic glioblastomas. In fact, the presence of both La and Ce at the site of the tumors (Figure 8b) indicated a positive response to radiotherapy, as well as the good stability of the nanoscintillators *in situ*. Therefore, this study was the first to show that LIBS imaging is beneficial for indirectly reflecting the efficacy of an anticancer treatment.

To keep up with radiotherapy improvements, LIBS imaging was also successfully used to establish that boron-containing fluorophores effectively reached tumors in a tumor-bearing chicken embryo model¹³³. In the context of boron neutron capture therapy (BNCT, an innovative radiotherapeutic modality based on neutrons), boron imaging truly represents one of the most promising application fields for LIBS, since this element is a very light chemical element and is therefore difficult to image with other elemental imaging modalities.

One of the most remarkable steps forward in the bioimaging of metal-NPs was the reporting of the intracellular localization of indium-based NPs with double-pulse LIBS technology¹²⁸. This was the first time that a LIBS imaging instrumentation setup successfully managed to surpass micrometer resolution for a biological sample (Figure 8c). In this study, Meng et al. used a nanolaser probe to improve the lateral resolution down to 500 nm. The combination of a femtosecond laser (515 nm for sampling) with a nanosecond laser (266 nm for emission enhancement) allowed the visualization of metal-NPs within single cells. Additionally, the indium elemental images exquisitely corresponded with the fluorescence images of lysosomes in cells, suggesting that these NPs enter the cells through endocytosis before being trapped in lysosomes. Not only did this inspirational study provide the first images of the subcellular distribution of metal-NPs in organelles, but with an absolute LoD of 18.3 fg, it

paved the way for exciting functional studies about the behaviors of and interactions between metal-NPs and cells.

In a study conducted on shark teeth (Figure 9a), fluorine imaging was performed through the spectral emission lines of the calcium fluoride (CaF) molecule¹³⁴. The strategy to indirectly analyze the distribution of an element via the use of molecular emission from plasma is very relevant and contradictory to the general dogma claiming that LIBS is efficient for analyzing chemical elements alone, without knowledge about the molecular information. The application of molecular emissions in LIBS is indeed a growing area of research¹³⁵, and we believe that there are many benefits to developing innovative LIBS imaging projects that also include molecular emission analysis. Recently, both elemental and molecular emissions were studied within a single project aiming at studying cancer in an animal model¹³⁶. In this work, melanoma cells were xenografted subcutaneously in mice. Once the tumors were excised, they were prepared for LIBS analysis, and the K elemental emission signals and CN molecular emission signal were selected for an algorithm-based discrimination between the melanoma and the surrounding nonmalignant dermis.

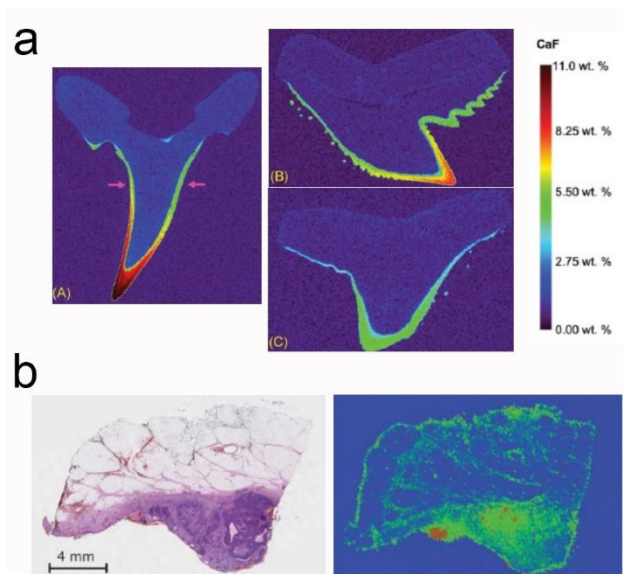


Figure 9: LIBS molecular imaging of shark teeth and LIBS elemental imaging in human skin tissues embedded in paraffin.

(a) CaF distribution in the teeth of the (A) sand tiger shark (with the cross-section location indicated by the red dashed line), (B) tiger shark, and (C) hammerhead shark using the 50 μm spot method. Reproduced from Determination of Fluorine Distribution in Shark Teeth by Laser Induced Breakdown Spectroscopy. Manard, B. T.; Hintz, C. J.; Quarles, C. D.; Burns, W.;

Zirakparvar, N. A.; Dunlap, D. R.; Beiswenger, T.; Cruz-Uribe, A. M.; Petrus, J. A.; Hexel, C. R., B. Manard, C. Hintz. *Metallomics* 2022, 14, mfac050 (ref ¹³⁴), with permission of Oxford University Press, CC BY license.

(b) Analysis of a basal-cell carcinoma: histological image (left) and Ca intensity map obtained with LIBS. Reproduced from Imaging margins of skin tumors using laser-induced breakdown spectroscopy and machine learning. K. Kiss, A. Sindelarova, L. Krbal, V. Stejskal, K. Mrazova, J. Vrabel, M. Kaska, P. Modlitbova, P. Porizka, J. Kaiser. *Journal of analytical Atomic Spectroscopy* 2021, 36, 909 (ref ¹³⁷), with permission from The Royal Society of Chemistry.

3.4.3 Elemental imaging of human tissue

The elemental analysis of human tissue is still a neglected area of research, especially because of the legislation and mandatory administrative procedures intrinsically linked to medical research involving human subjects, as defined by the Helsinki declaration from the World Medical Association¹³⁸. We must emphasize that every research protocol aiming at analyzing any kind of human fluid or human tissue is considered medical research, and investigators must conform to the Helsinki declaration by providing the ethics committee's approval number, as well as information regarding the written informed consent from patients. Several laboratories have developed projects aimed at improving cancer diagnosis, which is the most studied human pathology with LIBS. Most of these studies are performed with LIBS in a microanalytical setting, either on fluids (blood or serum) or tissues¹³⁹. We believe that spatial information is an important parameter, especially for studying solid cancer diseases in which tumor heterogeneity is key. Accordingly, we strongly encourage research teams to study solid malignancies with LIBS instruments tuned for elemental imaging, since the 2D spatial capability reflects the heterogeneous signals of tumors within their native environment. In a seminal work, Moncayo et al. studied the distribution of endogenous chemical elements (Na, P, Ca, Fe, Mg and Zn) in normal human skin, as well as in several different skin cancer types, such as malignant melanoma, squamous cell carcinoma, and Merkel cell carcinoma¹¹⁶. This descriptive approach allowed the obtainment of monoelemental images from human diseases, with a modest capacity to investigate differences between the elemental maps of normal versus cancer skin regions. In accordance with this work, another small series of human skin tissues was recently imaged with LIBS, and the distribution of several elements of interest (Na, K, Mg, and Ca) was

studied in a malignant melanoma, squamous cell carcinoma, basal cell carcinoma (Figure 9b) and hemangioma¹³⁷. This work also included the use of a self-organizing map (SOM) algorithm for clustering pixels according to elemental information. Another work aimed at studying the elemental distribution of elements (Ca, Mg, Na, C, Al, Fe, Si, and Cu) as well as molecular fragments (CN, C₂) in human lung specimens used a k-means algorithm to classify the elemental information of each pixel¹⁴⁰.

Notably, the first multicenter clinical trial with LIBS imaging has been registered¹⁴¹. This ongoing retrospective study aims to recruit 100 participating patients with lung diseases. The overall goal of this MEDICO-LIBS clinical study is to evaluate the feasibility of using LIBS imaging to identify, localize and possibly quantify metals within selected human specimens with idiopathic lung diseases. This study will generate massive databases that will necessitate the use of chemometric toolboxes to fully utilize the multidimensionality of the spectral information combined with the medico-biological information.

We believe that the use of chemometrics for treating such large datasets is key (please refer to the next paragraph) and will undeniably play a major future role in the LIBS imaging of human tissues. In addition, we anticipate great collaborations between LIBS imaging physicists and medical investigators. The former are in charge of developing instruments to image/quantify endogenous and exogenous elements with increased (nanoscale) resolution, and the latter are in charge of compliance with the ethical guidelines for medical research as well as for the choice of relevant specimens.

Regarding the different biomedical LIBS elemental imaging studies recently published, all studies focused on the semiquantitative information contained intrinsically in elemental images, and no absolute quantitative studies were performed. Several difficulties for calibration remain¹⁴², and we believe that the absolute concentrations of elements at the pixel level is not yet necessary for the proper clinical interpretation of elemental images. However, recent developments in calibration-free LIBS microanalysis¹⁴³ could lead to possible LIBS imaging applications, and we greatly encourage the scientific community to work on this promising challenge.

4. Data processing and chemometrics in LIBS imaging

To better understand the role of chemometrics in LIBS imaging today and to understand how it could evolve in the years to come, it is important to review the history of this spectroscopic imaging technique. Even if LIBS spectroscopy was, at the beginning, a technique for physicists who developed spectroscopic measurement systems, this technique has become a real analytical chemistry technique. Nevertheless, from our point of view, it is still not well known in the field, hence the need for this article. Similar to many other spectroscopic techniques, LIBS spectroscopy was first used for bulk analysis to investigate the presence of specific elements in complex samples. It has made its way into the industrial world for material characterization and has also become one of the flagship spectroscopic techniques in scientific research, having been installed on the Martian exploration rovers.

Hyperspectral LIBS imaging dates back to the 2000s, having exceptionally evolved and continuing to receive growing interest from all scientific communities, as this spectroscopic imaging technique has many interesting features. We will briefly discuss them here. First, this technique has a very high dynamic range allowing the detection of almost all elements from the percent to the ppm scale. It is also very fast with today's kHz acquisitions, i.e., it can acquire 1000 spectra per second with a spatial resolution of approximately 10 micrometers. In the 2000s, LIBS imaging datasets contained approximately 1000 pixels (i.e., 1000 spectra); they can now contain more than 10 million pixels, acquired in a few hours, for a sample exploration at the micron scale on a surface of several cm^2 . Each of these spectra is often made up of several thousands of wavelengths; such a dataset acquired on a sample exceeds several gigas of computer memory. As the LIBS spectrum presents fine and numerous emission lines, the researchers first generate a map of a given element by a simple integration of the signal measured at a supposedly specific wavelength of the element in question. It is the most commonly used method for many spectroscopic imaging techniques. Indeed, it is a simple and fast approach for generating elemental images from LIBS spectra, and it is quite natural that we continue to use it. We will see later in this section that researchers are still trying to improve this univariate use of data to better respond to the constraints and specificities of LIBS imaging. Nevertheless, we must not forget that the specificity of a chosen wavelength for a given element is a strong assumption. Indeed, even if a particularly thin emission line is chosen for the signal integration, the presence of many elements in the sample (some of them unexpected) each having a large number of emission

lines considerably increases the chances of an interference phenomenon. This results in overestimating the quantities of the element of interest for some spectra of the dataset and ultimately in biased distribution maps. Another aspect that may appear trivial, but which is of great importance in the exploration of spectral data, is that such a univariate methodology never produces maps for unexpected elements. In a way, we can even say that we ultimately exploit only a part of the information hidden in this dataset by generating chemical maps of preselected elements. We are not saying here that we should abandon this univariate approach of signal integration for generating chemical images. However, it is in our best interest to also use multivariate tools from chemometrics, which are able to simultaneously exploit the signal coming from all wavelengths of the spectral domain. We can thus attain a different and unbiased point of view of our spectral data. Above all, we have the possibility of extracting even more chemical information for an even more exhaustive exploitation and exploration of spectral imaging data. Nevertheless, we should not oppose the classical signal integration approach and multivariate chemometric methods because in fact, there are no incorrect approaches but rather incorrect interpretations of the results. It is therefore appropriate to use both techniques for LIBS imaging. The following paragraph gives an overview of the spectral data processing developed for LIBS imaging and the associated chemometric tools. We will therefore naturally exclude the works that used imaging instrumentation to acquire a large number of spectra, which were ultimately exploited in the form of a mean spectrum for bulk analysis, on a surface of interest.

First, regarding the classical integration method, the simplicity of this approach should not make us forget that precautions must be taken because it is not a push-button method. Motto-Ros et al.¹⁴⁴ proposed the statistical evaluation of three different signal integration methods to generate chemical images. They demonstrated that the values extracted by these different methods can generate very different maps while highlighting the most efficient map. More interestingly, the selected methodology allows the association of an uncertainty map to a generated elemental map. Therefore, it allows the evaluation of the veracity of the concentrations displayed for each pixel. Jolivet et al.⁸⁰ also used this approach to generate quantitative images of carbon in heterogeneous refining catalysts. Moreover, these images were used to estimate the LoD in this single-shot configuration, which is a very original concept.

If we return to a more general point of view, the heterogeneous character of the samples analyzed in LIBS imaging coupled with its great dynamics and good sensitivity often cause the saturation of certain emission bands in the acquired datasets. A saturation is a form of distortion that limits the signal once it exceeds a threshold. As a consequence, saturated bands with their characteristic plateaus present numerical values that do not correspond to the analytical reality of the analyzed sample. Any direct use of such data therefore leads to biased images. Unfortunately, it is not often possible to perform a second LIBS imaging experiment on the same area of a sample. The aim of a study by Nardecchia et al.¹⁴⁵ was to first show the importance of considering this phenomenon when analyzing spectral data at the risk of quickly creating artifacts in the generated images. Then, they proposed a method based on statistical imputation for correcting saturated bands. The concept was finally validated by considering a LIBS imaging dataset of a lung biopsy. It is noted that such a spectral correction can be done within the framework of the classical integration method but also prior to a chemometric method that we will introduce later. Let us now return in a general way to an elemental image obtained by the integration method. During a LIBS imaging experiment, we systematically acquire the spectra following a grid, and the area covered by the sample is often represented by a rectangle. We have seen that the integration method allowed us to obtain a value per position of spectral measurement that corresponded *in fine* to a colored pixel in the final map. Unfortunately, all these values are not significant from an analytical and statistical point of view, although they have been calculated. Sarah Richiero et al.¹⁴⁶ proposed a mask strategy to locate the pixels that should be kept in the image. This concept has been applied to the characterization of archaeological mortar. Additionally, the authors used image analysis tools to estimate the granulometry and the circularity of the aggregates from generated LIBS images. In the same perspective of LIBS image enhancement, Gimenez et al.⁶⁶ proposed a 3D image rendering method for better observing nanoparticle distributions in biological tissue.

Chemometrics offers many multivariate data analysis tools that have been used for a long time for other spectroscopic imaging techniques. It is therefore natural that the LIBS imaging community is interested in these tools. LIBS imaging has, however, a feature that other techniques do not have, namely, the massive nature of the acquired dataset that can contain several million spectra for a single sample. Thus, chemometricians are very interested in LIBS

imaging because they rarely encounter this type of massive spectroscopic data structure among the imaging techniques used in analytical chemistry. Of course, not all LIBS imaging experiments generate so many spectra, but when they do, some chemometrics algorithms must be revised to adapt to this specificity. In this case, the problem is not truly the computing capacity of our computers. We will now review all the methods in the chemometrics toolbox that have been used to enhance LIBS imaging datasets.

A hyperspectral imaging technique is primarily used to explore a partially unknown sample for which we only have the available spectra acquired over a certain region of interest. Therefore, it is quite natural that the first chemometric tools that were able to be used were unsupervised pattern recognition techniques. The best-known method in all spectroscopy fields is certainly PCA, which is the real Swiss Army knife of spectral data processing. Like all chemometrics algorithms, it is first a multivariate tool that simultaneously uses all the wavelengths of the spectral domain of interest, without any preconceived notion of the presumed importance of some of them. The analysis thus involves the extraction of principal components expressing the variances contained in the spectra. A component is analyzed in the form of a spectrum that allows the identification of different correlated or anti-correlated elements. This analysis also allows the generation of a score map associated with each component to observe the spatial distribution of the detected elements. It is a multivariate tool that is very simple to set up and use, allowing the initial chemical information of complex samples to be quickly obtained. Although it is not the subject here, it should be noted that PCA is often the core of more advanced chemometric methods. In their work, Moncayo et al.¹⁴⁷ used PCA to explore a dataset of more than two million spectra to characterize a complex mineral sample. They then showed how the chemical interpretation of principal components and score maps allowed the further characterization of major and minor mineral phases. This work was also an opportunity to show that such a chemometric analysis was possible considering the very large amount of data from LIBS imaging. *Sirven et al.*¹⁴⁸ have proposed a modification of this analysis called HyperPCA. It was developed with the objective of better managing particularly noisy data, which is quite common in LIBS imaging, and adapting to the sparse structure of LIBS data presenting numerous fine and often isolated lines.

The second approach, which is equally interesting in unsupervised analysis, is the so-called clustering method. Again here, we only have the spectra of the dataset available, and our

aim is to group all of them by similarities, i.e., include them in distinct groups of spectra called clusters. When this analysis is performed in the framework of LIBS imaging, we can create a map showing the spatial locations of these clusters in the sample region of interest. Kiss et al.¹³⁷ published a very interesting work on the application of clustering in histopathology. More precisely, a cluster analysis of LIBS imaging datasets acquired on skin samples allowed the margins of skin tumors to be defined. In other words, it was possible to highlight zones where the healthy and cancerous cells were located on the observed biological tissue without prior knowledge about it. While these clustering approaches can allow spectra to be grouped by similarity in a dataset, classical algorithms, such as *k-means*, are poorly suited to detecting major compounds, minor compounds or even traces simultaneously. In chemometrics, we say that we have an unbalanced dataset because there are potentially large differences in the number of spectra between major compounds, minor compounds and traces. Therefore, the *k-means* algorithm falls into the trap of extracting clusters that are not always representative of all the compounds present in the dataset and, moreover, does not always detect the compounds present in a low number of pixels. To answer this question, Nardecchia et al.¹⁴⁹ proposed a new method called *embedded k-means*. These authors proposed to first apply a *k-means* analysis on the whole dataset. The originality of this work also concerns the use of a criterion allowing the estimation of an optimal number of clusters. We must insist here on the fact that this number of clusters is always fixed *a priori*, which is not satisfactory for multivariate data exploration. As soon as this first set of clusters is fixed, a new *k-means* analysis is applied to each of the clusters containing a subset of spectra of the initial dataset. The optimum number of clusters is of course obtained by using the same criterion for each of them. In this way, we can say that it is a hierarchical *k-means* analysis with an automatic choice of the optimal number of clusters. This aforementioned paper showed the potential of this approach by applying it to the exploration of a LIBS dataset containing more than 2 million spectra from the analysis of a complex mineral sample. Indeed, they were able to observe both major and minor compounds as well as traces.

To conclude this section dedicated to unsupervised methods and based on the principle that exploratory methods such as PCA are poorly adapted to detect all the compounds of interest that may be present in a LIBS imaging set, we note that Wu et al.¹⁵⁰ developed a method called the *Interesting features finder* (IFF). The objective of this approach is to detect all the

compounds present in a spectral dataset independently of the variance that each of them could express. It is thus possible to detect a compound regardless of whether it is major, minor or even a trace present on a few pixels of a large LIBS dataset. The authors applied this concept to the exploration of a complex sample of aerosols collected in the Arctic and demonstrated that they were able to detect some completely invisible aerosols when using a conventional exploration tool such as the PCA.

Classification (also called *supervised pattern recognition*) is the second approach in the chemometric toolbox. The goal of such an approach is to build a model capable of predicting from a spectrum its membership to a group, also referred to as a class. Classification is often more difficult to employ in spectroscopic imaging because model construction and optimization require obtaining first a training dataset that will be composed of known spectrum/class pairs to establish this link. This explains the limited number of available publications on this topic (compared with those on unsupervised methods) as soon as spectroscopic imaging is considered. Here, we discuss the two main application fields of LIBS imaging today, namely, geology and biology. Regarding geology, Meima et al.¹⁵¹ applied the spectral angle mapper (SAM) algorithm for the supervised classification of imaging laser-induced breakdown spectroscopy (LIBS) data to investigate variations in the chemical/mineralogical compositions of complex ore on the submillimeter to the meter scale. For their part, Müller et al.¹⁵² used linear discriminant analysis (LDA) and semisupervised one-class support vector machines (OC-SVMs) to separate known minerals in geological drill cores based on a set of training samples while also detecting unknown material, i.e., new lithologies and/or minerals not in the training set. Regarding biology, Choi et al.¹⁵³ demonstrated that they were able to detect melanomas embedded in murine skin tissue using an SVM classification model.

The methodologies we have just discussed were, above all, qualitative, and it is quite natural that we now turn to quantitative LIBS imaging, an essential facet of analytical chemistry. We will, therefore, discuss regression methods and well-known approaches in the chemometrics toolbox. As a reminder, the aim of a regression method is to predict from a spectrum the concentration of a product of interest, and as for a classification, obtaining such a model will require first a training dataset, which will be composed of known spectrum/concentration pairs to establish this link. This approach is widely used in LIBS spectroscopy for bulk analysis. However, LIBS imaging remains very anecdotal because of the difficulty of obtaining

concentrations from a reference method in this specific framework. It is in the agri-food domain that we find the use of the well-known partial least squares (PLS) regression for the estimation of quantitative maps for the analysis of beef meat^{154,155} or infant formula samples¹⁵⁶.

The third type of approach we can find in the chemometric toolbox is signal unmixing. This technique is particular, since it is both a qualitative and quantitative method, hence our desire to introduce it separately from the previous sections. It is indeed, first of all, an unsupervised method that works only on spectra contained in an imaging dataset without any prior knowledge about them. In other words, it is potentially a good exploration technique. On the other hand, the goal of such a method is to simultaneously extract the pure spectra of all the compounds present in the dataset and also give their relative concentrations within each individual spectrum. At the end of such a procedure, we obtain for each compound present in the sample a pure spectrum used for its identification associated with its chemical distribution map. It is then possible to detect a chemical compound that is not expected and also observe its spatial distribution in the sample, which is quite a new ability compared to the abilities of other chemometric tools. The multivariate curve resolution-alternating least squares (MCR-ALS) method is certainly the most commonly used method in chemometrics for signal unmixing. This is also the case in LIBS imaging, as shown by the work of Sandoval-Munoz et al.¹⁵⁷ and El Haddad et al.¹⁵⁸, for the characterization of complex mineral samples. Nardecchia et al.¹⁵⁹ also used the MCR-ALS method to simultaneously explore two imaging datasets of the same mineral sample from LIBS and plasma-induced photoluminescence (PIL). This was the first time that such a data fusion approach was proposed to further the understanding of the still poorly known luminescence phenomenon of complex samples. This study was also an opportunity to propose a double data compression strategy to make MCR-ALS calculations possible for a dataset of more than 2 million LIBS/PIL spectral pairs.

We will now conclude this discussion of the chemometric toolbox used in LIBS imaging by looking at neural networks, which, like the previous methods, can be used for exploration or prediction purposes. Based on the premise that nonlinear phenomena are potentially present in LIBS spectroscopic measurements, researchers have used neural networks in bulk analysis to predict concentrations from the beginning of analytical implementations. We must say that their use in the LIBS imaging field has been very limited. Thus, Pagnotta et

al.¹⁶⁰ used self-organizing maps (SOM) for the study of ancient Roman mortars using LIBS imaging. These neural networks, also called Kohonen maps, are named after their inventor, allowing nonlinear projections of these spectral data. In this work, the generated maps were then used for clustering. In a second paper, Pagnotta et al.¹⁶¹ coupled Kohonen maps with calibration-free LIBS (CF-LIBS) for the quantification on the same kind of sample. While classical neural networks (consisting of an input layer, a hidden layer and an output layer) have never been used in LIBS imaging, the first applications of deep neural networks are appearing in the field. These networks have many layers of interconnected neurons that are particularly suitable for exploiting spatial image characteristics. The advent of such networks has of course only been possible through the development of new learning strategies as the number of parameters (i.e., weights of the neurons) for optimizing these structures has become impressive. Chen et al.¹⁶² used a convolutional neural network (CNN) to classify rocks from elemental images that were obtained by the classical signal integration method. In consideration of the limited size of the training dataset in relation to the very large number of weights of the network to be optimized, the authors have rightly proposed data augmentation strategies in order to avoid the over-training of such a network, a situation still too often observed in many publications in analytical chemistry. This deep learning approach has also been compared to a support vector machine (SVM), another well-known nonlinear classification approach in chemometrics.

In conclusion, there are, for the moment, relatively few publications presenting the use or development of multivariate tools for the processing of spectral data from LIBS imaging experiments, contrary to other imaging techniques, such as vibrational spectroscopy. As we have already seen in this last scientific domain, and from our point of view, things will accelerate very quickly in LIBS imaging, with a significant increase in publications in the coming years. Indeed, the LIBS community is now aware of the potential of such approaches that allow us to even further investigate complex samples using a hyperspectral LIBS imaging dataset in a different way. Digital pressure will also contribute to this acceleration. Indeed, today, a LIBS imaging dataset acquired from a sample can contain more than 10 million spectra, and it is obvious that the integration method alone does not allow us to see below the tip of the figurative iceberg. However, we must admit that even if chemometrics has many multivariate methods in its toolbox, they are not necessarily applicable when such a large amount of data has to be considered. To respond to this new constraint, we will have

to find ingenious methodologies allowing us to continue to use these tools or even to revise them completely. Finally, this evolution of chemometrics in LIBS imaging will be all the more rapid as researchers propose open-access codes and software so that we can all do our own experiments and increase our skills without having to write code, which is, of course, not necessarily our expertise.

5. Conclusion

LIBS imaging is currently strongly developing, with a significant increase in the number of articles published in recent years. Thanks to the studies carried out in the laboratory on methodological, instrumental and applicative development, this approach is becoming progressively more mature, and it is now identified as a good candidate to become, in the near future, a reference technique for spatially resolved elemental characterization. An increasing number of companies are currently working on the development of reliable, accurate and robust commercial instruments, gradually opening up the possibility of disseminating the technique to a larger number of users, particularly in the field of analytical sciences. As mentioned above, LIBS imaging indeed has unique features, such as a micrometer-scale resolution with detection limits down to the ppm scale, fast operating speed (up to kHz), large surface area analyzed (tens to hundreds of cm²), and ambient operating conditions with all-optical benchtop instrumentation. To top it all off, the greatest strength of LIBS imaging is undoubtedly its ability to detect light elements with excellent sensitivities down to a hundred ppb. This makes it very complementary to more standard spectroscopic techniques, such as LA-ICP-MS and/or micro-XRF.

As we have seen in this review, LIBS imaging has many advantages that should allow it to become a full-fledged analytical technique very soon. What is certain is that at some point, its development will have to be supported by private companies. In addition, as already discussed, efforts will have to be made to facilitate the data processing stage. The high spectral complexity, as well as the large amount of data to be processed (easily reaching one million spectra per cm²), currently requires significant expertise to extract all the relevant information contained in the datasets. This expertise does not stop at this point because it is also necessary to detect possible measurement artifacts (self-absorption, spectral

interference, etc.) at the risk of generating distribution maps not representative of the analytical reality of the sample. This aspect tends to slow down the development and diffusion of LIBS imaging as a routine technique since it remains dependent on the spectroscopic expertise of the analyst. Aligned with this, the use of chemometric tools opens up highly relevant avenues of progress. However, these are not yet fully generalized, and research on this topic is still needed to fully understand the capabilities of these approaches. The application of new processing concepts and the management of a large volume of data allows us to imagine new analytical strategies for LIBS imaging in the short term; why not eventually use artificial intelligence for fully automated treatment? This type of tool would be perfectly adapted, even allowing real-time processing, but its implementation would require rigorous and very advanced developments.

In addition, there are other relevant aspects that would require further research. First, we can mention the detection of halogen elements that suffer from poor detectability in LIBS (LoD~%). The possibility of detecting these elements indirectly through the detection of the stronger molecular emission of radicals, such as CaF or CaCl (etc...), opens up very interesting avenues^{163,164}. However, to adapt this method to LIBS imaging, it is necessary to further develop strategies to ensure a reproducible and controllable formation of these radicals in plasma, compensating for the inhomogeneity of the alkaline earth elements in the samples by further developing the existing methodologies in this regard. Furthermore, and with the idea of improving the sensitivity of the technique for certain categories of elements, the use of plasma as a source of excitation for luminescence measurements seems interesting for the detection of REEs. This approach, known as plasma-induced luminescence (PIL), offers low LoDs (typically <ppm) for various REE elements, such as europium (Eu), samarium (Sm), dysprosium (Dy), gadolinium (Gd), or praseodymium (Pr), while using the same instrumentation^{104,165} but covering larger delays (typically >100 μ s). Finally, the analysis of complex materials (i.e., composed of several matrices) still appears challenging in terms of quantification. As discussed above, the use of complementary techniques, such as EPMA or LA-ICP-MS, allows the efficient calibration of LIBS signals. However, these approaches are time-consuming to implement, and the community needs to develop more efficient calibration methods. Further studies need to be conducted to improve the quantification capabilities of LIBS imaging, either through the development of different

reference samples or through the application of methodologies, where the use of CF-LIBS and related methods represents an interesting opportunity.

Biographies

Benoit Busser is a senior medical biochemist in Grenoble Hospital and an Associate Professor in Biochemistry at the Faculty of Pharmacy, Grenoble Alpes University, France.

He studied pharmaceutical sciences in Strasbourg and performed his residency in Grenoble, Hospital (PharmD in 2008). Additionally, he received his PhD in cellular biology and cancer sciences in Grenoble in 2009. He was first appointed as an assistant professor in 2009 and then as an associate professor in 2012 (university-hospital dual position). He led the cancer clinical laboratory of Grenoble Hospital for 3 years, and in 2017, he joined the Light and Matter Institute (ILM) in Lyon for a 1-year research mobility dedicated to the development of the LIBS multielemental imaging of human specimens. He received the prestigious “Young Investigator Award” in 2015 from the European Society of Molecular Imaging (ESMI) and was appointed as a member of the Institut Universitaire de France (IUF) in 2021.

He is now the leader of the "elemental pathology group" at the Institute for Advanced Biosciences in Grenoble, and his current research activities include (1) exploring the fate of metal nanoparticles with therapeutic interest, (2) studying anticancer drug resistance mechanisms, and (3) characterizing the endogenous or exogenous (exposure-related) elemental content of healthy/diseased tissues with LIBS.

Vincent Motto-Ros graduated in Physics in December 2005 at University Claude Bernard Lyon 1 (Lyon, France). After two postdoctoral positions at the Canadian Space Agency (Montréal, Quebec) and at the Liphy Laboratory (Grenoble, France), he obtained an associate professor position at the University Claude Bernard Lyon 1 in 2008. Since then, he has been working on the development of the LIBS technique at the Light and Matter Institute (ILM). He has excellent international visibility for his expertise in LIBS instrumental development, quantification, experimental training, and the elemental imaging of biological tissues. He is the author of more than 100 papers in peer reviewed journals, with 2 patents, approximately 70 presentations at national and international conferences, and 40 invited talks/lectures at international conferences. He has more than 3800 total citations and an H-index=39 (Google Scholar).

Vincent Gardette graduated with a master's degree in Climate Science at Lyon 1 University and then obtained his PhD in Chemistry at the University of Bari in 2022. He is currently working as a Post Doc at the Light and Matter Institute (ILM) in Lyon. His research focuses on LIBS imaging applications, especially in the medical field, and also the fundamentals of laser ablation, laser-matter interactions and plasma physics.

Ludovic Duponchel defended his PhD in Physical Chemistry in 1997 at the University of Lille (France). His research was focused on the development of a portable near-infrared spectrometer for chemical analysis in the agrofood industry. During this period, he spent two years in the Horiba Jobin-Yvon Company in Paris performing instrumental and chemometrics research. He was then first recruited as an Assistant Professor at the University of Lille in 1998 and then as a Full Professor in 2008. His academic interests focus on the development of new chemometric methodologies to further explore various kinds of datasets considering different spectroscopies and instrumental configurations, particularly in the hyperspectral imaging framework. This research was performed in the LASIRE laboratory (University of Lille). He has been the Chairman of the French Chemometrics Society under the aegis of the French Statistical Society since 2013.

Lucie Sancey has been Director of Research of the French CNRS at the Institute for Advanced Biosciences since 2020 in Grenoble, France. Her research activities focus on the development and evaluation of innovative compounds for cancer imaging and treatment. This includes the development of nanoagents for cancer diagnosis and therapy, particularly for new multimodal optical contrast agents and new imaging techniques for biological tissues, including fluorophores for image-guided surgery. Having been a researcher at the Light and Matter Institute (ILM) in Lyon from 2012 to 2016, she contributed to the early development of LIBS for the multielemental imaging of biological tissues. She is the author of more than 90 scientific communications; she co-founded 2 start-ups and holds 2 patents. She is a board member of SFNano (the French Society of Nanomedicine), a member of the German BNCT Society (DGBNCT), a member of the French research group "Nuclear Methods and Tools against Cancer" and a member of the scientific steering committee of the Cancéropôle Lyon Auvergne Rhône-Alpes for the thematic axis "Innovative Technology for Health".

Dr. César Alvarez Llamas received his BSc in Physics in 2011 and his MSc in Analytical Chemistry at University of Oviedo, Spain in 2012. He received his PhD in Physics (Hons.) in 2017 working on the laser-induced breakdown spectroscopy (LIBS) technique. As a Postdoc, he studied portable LIBS equipment at the Carnot Interdisciplinary Laboratory Burgundy (ICB), Dijon, France; the analysis of collimated nanoparticles in Commissariat à l'énergie atomique et aux énergies alternatives (CEA), Saclay, France; and the use of LIBS together with acoustic signals for Mars geo-exploration applications under the NASA Mars 2020 mission in UMALASERLAB (Univ. of Málaga, Spain). He is currently working on the applications of kHz LIBS at the Institute Light and Matter (ILM), Lyon, France.

Acknowledgements

This work was partially supported by the French region Auvergne Rhône-Alpes (Optolyse, CPER2016), and two French ANR grants (ANR-17-CE18-0028 “MEDI-LIBS” and ANR-20-CE17-0021 “dIAG-EM”). In addition, we gratefully acknowledge Dr. Frédéric Pelascini from Cétim Grand Est, Dr. Florian Trichard from Ablatom SAS, Dr. Sylvain Hermelin and Professor Christophe Dujardin from the Light and Matter Institute (ILM) for fruitful discussions. We would also like to acknowledge the professional manuscript services of Springer Nature Author Services.

References

- (1) Piñon, V.; Mateo, M. P.; Nicolas, G. Laser-Induced Breakdown Spectroscopy for Chemical Mapping of Materials. *Appl. Spectrosc. Rev.* **2013**, *48* (5), 357–383. <https://doi.org/10.1080/05704928.2012.717569>.
- (2) Jolivet, L.; Leprince, M.; Moncayo, S.; Sorbier, L.; Lienemann, C.-P.; Motto-Ros, V. Review of the Recent Advances and Applications of LIBS-Based Imaging. *Spectrochim. Acta Part B At. Spectrosc.* **2019**, *151*, 41–53. <https://doi.org/10.1016/j.sab.2018.11.008>.
- (3) Busser, B.; Moncayo, S.; Coll, J.-L.; Sancey, L.; Motto-Ros, V. Elemental Imaging Using Laser-Induced Breakdown Spectroscopy: A New and Promising Approach for Biological and Medical Applications. *Coord. Chem. Rev.* **2018**, *358*, 70–79. <https://doi.org/10.1016/j.ccr.2017.12.006>.
- (4) Gaudio, R.; Melikechi, N.; Abdel-Salam, Z. A.; Harith, M. A.; Palleschi, V.; Motto-Ros, V.; Busser, B. Laser-Induced Breakdown Spectroscopy for Human and Animal Health: A Review. *Spectrochim. Acta Part B At. Spectrosc.* **2019**, *152*, 123–148. <https://doi.org/10.1016/j.sab.2018.11.006>.
- (5) Limbeck, A.; Brunnbauer, L.; Lohninger, H.; Pořizka, P.; Modlitbová, P.; Kaiser, J.; Janovszky, P.; Kéri, A.; Galbács, G. Methodology and Applications of Elemental Mapping by Laser Induced Breakdown Spectroscopy. *Anal. Chim. Acta* **2021**, *1147*, 72–98. <https://doi.org/10.1016/j.aca.2020.12.054>.
- (6) Sancey, L.; Motto-Ros, V.; Busser, B.; Kotb, S.; Benoit, J. M.; Piednoir, A.; Lux, F.; Tillement, O.; Panczer, G.; Yu, J. Laser Spectrometry for Multi-Elemental Imaging of Biological Tissues. *Sci Rep* **2014**, *4*, 6065. <https://doi.org/10.1038/srep06065>.
- (7) Cáceres, J. O.; Pelascini, F.; Motto-Ros, V.; Moncayo, S.; Trichard, F.; Panczer, G.; Marín-Roldán, A.; Cruz, J. A.; Coronado, I.; Martín-Chivelet, J. Megapixel Multi-Elemental Imaging by Laser-Induced Breakdown Spectroscopy, a Technology with Considerable Potential for Paleoclimate Studies. *Sci. Rep.* **2017**, *7* (1), 5080. <https://doi.org/10.1038/s41598-017-05437-3>.
- (8) Janssens, K.; De Nolf, W.; Van Der Snickt, G.; Vincze, L.; Vekemans, B.; Terzano, R.; Brenker, F. E. Recent Trends in Quantitative Aspects of Microscopic X-Ray Fluorescence Analysis. *TrAC Trends Anal. Chem.* **2010**, *29* (6), 464–478. <https://doi.org/10.1016/j.trac.2010.03.003>.
- (9) Moore, K. L.; Lombi, E.; Zhao, F.-J.; Grovenor, C. R. M. Elemental Imaging at the Nanoscale: NanoSIMS and Complementary Techniques for Element Localisation in Plants. *Anal. Bioanal. Chem.* **2012**, *402* (10), 3263–3273. <https://doi.org/10.1007/s00216-011-5484-3>.
- (10) Pozebon, D.; Scheffler, G. L.; Dressler, V. L.; Nunes, M. A. G. Review of the Applications of Laser Ablation Inductively Coupled Plasma Mass Spectrometry (LA-ICP-MS) to the Analysis of Biological Samples. *J. Anal. At. Spectrom.* **2014**, *29* (12), 2204–2228. <https://doi.org/10.1039/C4JA00250D>.
- (11) Reich, M.; Large, R.; Deditius, A. P. New Advances in Trace Element Geochemistry of Ore Minerals and Accessory Phases. *Ore Geol. Rev.* **2017**, *81*, 1215–1217. <https://doi.org/10.1016/j.oregeorev.2016.10.020>.
- (12) Baudalet, M.; Smith, B. W. The First Years of Laser-Induced Breakdown Spectroscopy. *J. Anal. At. Spectrom.* **2013**, *28* (5), 624–629. <https://doi.org/10.1039/C3JA50027F>.

- (13) Moenke, H.; Moenke-Blankenburg, L. *Laser Micro-Spectrochemical Analysis*; Hilger: London, 1973.
- (14) Menut, D.; Fichet, P.; Lacour, J.-L.; Rivoallan, A.; Mauchien, P. Micro-Laser-Induced Breakdown Spectroscopy Technique: A Powerful Method for Performing Quantitative Surface Mapping on Conductive and Nonconductive Samples. *Appl. Opt.* **2003**, *42*, 6063–6071. <https://doi.org/10.1364/AO.42.006063>.
- (15) Bette, H.; Noll, R. High Speed Laser-Induced Breakdown Spectrometry for Scanning Microanalysis. *J. Phys. Appl. Phys.* **2004**, *37* (8), 1281. <https://doi.org/10.1088/0022-3727/37/8/018>.
- (16) Lucena, P.; Vadillo, J. M.; Laserna, J. J. Mapping of Platinum Group Metals in Automotive Exhaust Three-Way Catalysts Using Laser-Induced Breakdown Spectrometry. *Anal. Chem.* **1999**, *71* (19), 4385–4391. <https://doi.org/10.1021/ac9902998>.
- (17) Romero, D.; Laserna, J. J. Multielemental Chemical Imaging Using Laser-Induced Breakdown Spectrometry. *Anal. Chem.* **1997**, *69* (15), 2871–2876. <https://doi.org/10.1021/ac9703111>.
- (18) Lucena, P.; Laserna, J. J. Three-Dimensional Distribution Analysis of Platinum, Palladium and Rhodium in Auto Catalytic Converters Using Imaging-Mode Laser-Induced Breakdown Spectrometry. *Spectrochim. Acta Part B At. Spectrosc.* **2001**, *56* (2), 177–185. [https://doi.org/10.1016/S0584-8547\(00\)00298-6](https://doi.org/10.1016/S0584-8547(00)00298-6).
- (19) Motto-Ros, V.; Sancey, L.; Wang, X. C.; Ma, Q. L.; Lux, F.; Bai, X. S.; Panczer, G.; Tillement, O.; Yu, J. Mapping Nanoparticles Injected into a Biological Tissue Using Laser-Induced Breakdown Spectroscopy. *Spectrochim. Acta Part B At. Spectrosc.* **2013**, *87*, 168–174. <https://doi.org/10.1016/j.sab.2013.05.020>.
- (20) Motto-Ros, V.; Sancey, L.; Ma, Q. L.; Lux, F.; Bai, X. S.; Wang, X. C.; Yu, J.; Panczer, G.; Tillement, O. Mapping of Native Inorganic Elements and Injected Nanoparticles in a Biological Organ with Laser-Induced Plasma. *Appl. Phys. Lett.* **2012**, *101* (22), 223702. <https://doi.org/10.1063/1.4768777>.
- (21) Sancey, L.; Motto-Ros, V.; Kotb, S.; Wang, X.; Lux, F.; Panczer, G.; Yu, J.; Tillement, O. Laser-Induced Breakdown Spectroscopy: A New Approach for Nanoparticle's Mapping and Quantification in Organ Tissue. *J. Vis. Exp. JoVE* **2014**, No. 88. <https://doi.org/10.3791/51353>.
- (22) Moncayo, S.; Duponchel, L.; Mousavipak, N.; Panczer, G.; Trichard, F.; Bousquet, B.; Pelascini, F.; Motto-Ros, V. Exploration of Megapixel Hyperspectral LIBS Images Using Principal Component Analysis. *J. Anal. At. Spectrom.* **2018**, *33* (2), 210–220. <https://doi.org/10.1039/C7JA00398F>.
- (23) Bassel, L.; Motto-Ros, V.; Trichard, F.; Pelascini, F.; Ammari, F.; Chapoulie, R.; Ferrier, C.; Lacanette, D.; Bousquet, B. Laser-Induced Breakdown Spectroscopy for Elemental Characterization of Calcitic Alterations on Cave Walls. *Environ. Sci. Pollut. Res.* **2017**, *24* (3), 2197–2204. <https://doi.org/10.1007/s11356-016-7468-5>.
- (24) Fabre, C. Advances in Laser-Induced Breakdown Spectroscopy Analysis for Geology: A Critical Review. *Spectrochim. Acta Part B At. Spectrosc.* **2020**, *166*, 105799. <https://doi.org/10.1016/j.sab.2020.105799>.
- (25) Motto-Ros, V.; Moncayo, S.; Fabre, C.; Busser, B. Chapter 14 - LIBS Imaging Applications. In *Laser-Induced Breakdown Spectroscopy (Second Edition)*; Singh, J. P., Thakur, S. N., Eds.; Elsevier: Amsterdam, 2020; pp 329–346. <https://doi.org/10.1016/B978-0-12-818829-3.00014-9>.

- (26) Zhao, C.; Dong, D.; Du, X.; Zheng, W. In-Field, In Situ, and In Vivo 3-Dimensional Elemental Mapping for Plant Tissue and Soil Analysis Using Laser-Induced Breakdown Spectroscopy. *Sensors* **2016**, *16* (10), 1764. <https://doi.org/10.3390/s16101764>.
- (27) Krajcarová, L.; Novotný, K.; Kummerová, M.; Dubová, J.; Gloser, V.; Kaiser, J. Mapping of the Spatial Distribution of Silver Nanoparticles in Root Tissues of Vicia Faba by Laser-Induced Breakdown Spectroscopy (LIBS). *Talanta* **2017**, *173*, 28–35. <https://doi.org/10.1016/j.talanta.2017.05.055>.
- (28) Lednev, V.; Sdvizhenskii, P.; Grishin, M.; Cheverikin, V.; Stavertiy, A.; Tretyakov, R.; Taksanc, M.; Pershin, S. Laser-Induced Breakdown Spectroscopy for Three-Dimensional Elemental Mapping of Composite Materials Synthesized by Additive Technologies. *Appl. Opt.* **2017**, *56*, 9698. <https://doi.org/10.1364/AO.56.009698>.
- (29) Rifai, K.; Constantin, M.; Yilmaz, A.; Ozcan, L.; Doucet, F.; Azami, N. Quantification of Lithium and Mineralogical Mapping in Crushed Ore Samples Using Laser Induced Breakdown Spectroscopy. *Minerals* **2022**, *12*, 253. <https://doi.org/10.3390/min12020253>.
- (30) Rifai, K.; Doucet, F.; Özcan, L.; Vidal, F. LIBS Core Imaging at KHz Speed: Paving the Way for Real-Time Geochemical Applications. *Spectrochim. Acta Part B At. Spectrosc.* **2018**, *150*, 43–48. <https://doi.org/10.1016/j.sab.2018.10.007>.
- (31) Rifai, K.; Özcan, L.; Doucet, F.; Vidal, F. Quantification of Copper, Nickel and Other Elements in Copper-Nickel Ore Samples Using Laser-Induced Breakdown Spectroscopy. *Spectrochim. Acta Part B At. Spectrosc.* **2020**, *165*, 105766. <https://doi.org/10.1016/j.sab.2020.105766>.
- (32) Rifai, K.; Michaud Paradis, M.-C.; Swierczek, Z.; Doucet, F.; Özcan, L.; Fayad, A.; Li, J.; Vidal, F. Emergences of New Technology for Ultrafast Automated Mineral Phase Identification and Quantitative Analysis Using the CORIOSITY Laser-Induced Breakdown Spectroscopy (LIBS) System. *Minerals* **2020**, *10* (10), 918. <https://doi.org/10.3390/min10100918>.
- (33) Paradis, M.-C. M.; Doucet, F. R.; Rifai, K.; Özcan, L. Ç.; Azami, N.; Vidal, F. ECORE: A New Fast Automated Quantitative Mineral and Elemental Core Scanner. *Minerals* **2021**, *11* (8), 859. <https://doi.org/10.3390/min11080859>.
- (34) Motto-Ros, V.; Gardette, V.; Leprince, M.; Genty, D.; Sancey, L.; Roux, S.; Busser, B.; Pelascini, F. LIBS-Based Imaging: Recent Advances and Future Directions. *Spectroscopy* **2020**, *35* (2), 34–40.
- (35) Bai, X.; Ma, Q.; Motto-Ros, V.; Yu, J.; Sabourdy, D.; Nguyen, L.; Jalocha, A. Convoluting Effect of Laser Fluence and Pulse Duration on the Property of a Nanosecond Laser-Induced Plasma into an Argon Ambient Gas at the Atmospheric Pressure. *J. Appl. Phys.* **2013**, *113* (1), 013304. <https://doi.org/10.1063/1.4772787>.
- (36) Motto-Ros, V.; Negre, E.; Pelascini, F.; Panczer, G.; Yu, J. Precise Alignment of the Collection Fiber Assisted by Real-Time Plasma Imaging in Laser-Induced Breakdown Spectroscopy. *Spectrochim. Acta Part B At. Spectrosc.* **2014**, *92*, 60–69. <https://doi.org/10.1016/j.sab.2013.12.008>.
- (37) Hai, R.; Li, C.; Wang, H.; Ding, H.; Zhuo, H.; Wu, J.; Luo, G.-N. Characterization of Li Deposition on the First Wall of EAST Using Laser-Induced Breakdown Spectroscopy. *J. Nucl. Mater.* **2013**, *438*, S1168–S1171. <https://doi.org/10.1016/j.jnucmat.2013.01.258>.
- (38) Li, C.; Wu, X.; Zhang, C.; Ding, H.; Hu, J.; Luo, G.-N. In Situ Chemical Imaging of Lithiated Tungsten Using Laser-Induced Breakdown Spectroscopy. *J. Nucl. Mater.* **2014**, *452* (1–3), 10–15. <https://doi.org/10.1016/j.jnucmat.2014.04.041>.

- (39) Ahamer, C. M.; Riepl, K. M.; Huber, N.; Pedarnig, J. D. Femtosecond Laser-Induced Breakdown Spectroscopy: Elemental Imaging of Thin Films with High Spatial Resolution. *Spectrochim. Acta Part B At. Spectrosc.* **2017**, *136*, 56–65. <https://doi.org/10.1016/j.sab.2017.08.005>.
- (40) Wang, X.; Liang, Z.; Meng, Y.; Wang, T.; Hang, W.; Huang, B. Sub-Microanalysis of Solid Samples with near-Field Enhanced Atomic Emission Spectroscopy. *Spectrochim. Acta Part B At. Spectrosc.* **2018**, *141*, 1–6. <https://doi.org/10.1016/j.sab.2017.12.008>.
- (41) Giannakaris, N.; Haider, A.; Ahamer, C. M.; Grünberger, S.; Trautner, S.; Pedarnig, J. D. Femtosecond Single-Pulse and Orthogonal Double-Pulse Laser-Induced Breakdown Spectroscopy (LIBS): Femtogram Mass Detection and Chemical Imaging with Micrometer Spatial Resolution. *Appl. Spectrosc.* **2022**, *76* (8), 926–936. <https://doi.org/10.1177/00037028211042398>.
- (42) Jantzi, S. C.; Motto-Ros, V.; Trichard, F.; Markushin, Y.; Melikechi, N.; De Giacomo, A. Sample Treatment and Preparation for Laser-Induced Breakdown Spectroscopy. *Spectrochim. Acta Part B At. Spectrosc.* **2016**, *115*, 52–63. <https://doi.org/10.1016/j.sab.2015.11.002>.
- (43) Barnett, C.; Cahoon, E.; Almirall, J. R. Wavelength Dependence on the Elemental Analysis of Glass by Laser Induced Breakdown Spectroscopy. *Spectrochim. Acta Part B At. Spectrosc.* **2008**, *63* (10), 1016–1023. <https://doi.org/10.1016/j.sab.2008.07.002>.
- (44) Fornarini, L.; Spizzichino, V.; Colao, F.; Fantoni, R.; Lazic, V. Influence of Laser Wavelength on LIBS Diagnostics Applied to the Analysis of Ancient Bronzes. *Anal. Bioanal. Chem.* **2006**, *385* (2), 272–280. <https://doi.org/10.1007/s00216-006-0300-1>.
- (45) Guerra, M. B. B.; Adame, A.; Almeida, E. de; Carvalho, G. G. A. de; Brasil, M. A. S.; Jr, D. S.; Krug, F. J. Direct Analysis of Plant Leaves by EDXRF and LIBS: Microsampling Strategies and Cross-Validation. *J. Anal. At. Spectrom.* **2015**, *30* (7), 1646–1654. <https://doi.org/10.1039/C5JA00069F>.
- (46) Hou, H.; Cheng, L.; Richardson, T.; Chen, G.; Doeff, M.; Zheng, R.; Russo, R.; Zorba, V. Three-Dimensional Elemental Imaging of Li-Ion Solid-State Electrolytes Using Fs-Laser Induced Breakdown Spectroscopy (LIBS). *J. Anal. At. Spectrom.* **2015**, *30* (11), 2295–2302. <https://doi.org/10.1039/C5JA00250H>.
- (47) Lefebvre, C.; Catalá-Espí, A.; Sobron, P.; Koujelev, A.; Léveillé, R. Depth-Resolved Chemical Mapping of Rock Coatings Using Laser-Induced Breakdown Spectroscopy: Implications for Geochemical Investigations on Mars. *Planet. Space Sci.* **2016**, *126*, 24–33. <https://doi.org/10.1016/j.pss.2016.04.003>.
- (48) Schiavo, C.; Menichetti, L.; Grifoni, E.; Legnaioli, S.; Lorenzetti, G.; Poggialini, F.; Pagnotta, S.; Palleschi, V. High-Resolution Three-Dimensional Compositional Imaging by Double-Pulse Laser-Induced Breakdown Spectroscopy. *J. Instrum.* **2016**, *11* (08), C08002–C08002. <https://doi.org/10.1088/1748-0221/11/08/C08002>.
- (49) Noll, R.; Bette, H.; Brysch, A.; Kraushaar, M.; Mönch, I.; Peter, L.; Sturm, V. Laser-Induced Breakdown Spectrometry - Applications for Production Control and Quality Assurance in the Steel Industry. *Spectrochim. Acta Part B At. Spectrosc.* **2001**, *56* (6), 637–649. [https://doi.org/10.1016/S0584-8547\(01\)00214-2](https://doi.org/10.1016/S0584-8547(01)00214-2).
- (50) Boué-Bigne, F. Laser-Induced Breakdown Spectroscopy Applications in the Steel Industry: Rapid Analysis of Segregation and Decarburization. *Spectrochim. Acta Part B At. Spectrosc.* **2008**, *63* (10), 1122–1129. <https://doi.org/10.1016/j.sab.2008.08.014>.

- (51) Boué-Bigne, F. Simultaneous Characterization of Elemental Segregation and Cementite Networks in High Carbon Steel Products by Spatially-Resolved Laser-Induced Breakdown Spectroscopy. *Spectrochim. Acta Part B At. Spectrosc.* **2014**, *96*, 21–32. <https://doi.org/10.1016/j.sab.2014.03.011>.
- (52) Manard, B. T.; Quarles, C. D.; Wylie, E. M.; Xu, N. Laser Ablation – Inductively Couple Plasma – Mass Spectrometry/Laser Induced Break down Spectroscopy: A Tandem Technique for Uranium Particle Characterization. *J. Anal. At. Spectrom.* **2017**, *32* (9), 1680–1687. <https://doi.org/10.1039/C7JA00102A>.
- (53) Sweetapple, M. T.; Tassios, S. Laser-Induced Breakdown Spectroscopy (LIBS) as a Tool for in Situ Mapping and Textural Interpretation of Lithium in Pegmatite Minerals. *Am. Mineral.* **2015**, *100* (10), 2141–2151. <https://doi.org/10.2138/am-2015-5165>.
- (54) López-López, M.; Alvarez-Llamas, C.; Pisonero, J.; García-Ruiz, C.; Bordel, N. An Exploratory Study of the Potential of LIBS for Visualizing Gunshot Residue Patterns. *Forensic Sci. Int.* **2017**, *273*, 124–131. <https://doi.org/10.1016/j.forsciint.2017.02.012>.
- (55) Rakovský, J.; Musset, O.; Buoncristiani, J.; Bichet, V.; Monna, F.; Neige, P.; Veis, P. Testing a Portable Laser-Induced Breakdown Spectroscopy System on Geological Samples. *Spectrochim. Acta Part B At. Spectrosc.* **2012**, *74–75*, 57–65. <https://doi.org/10.1016/j.sab.2012.07.018>.
- (56) Beresko, C.; Dietz, T.; Kohns, P.; Ankerhold, G. Schnelle Materialanalyse mit Lasern: Neue Möglichkeiten durch 3D-LIBS und Raman-Spektroskopie. *Tm - Tech. Mess.* **2014**, *81* (11), 537–545. <https://doi.org/10.1515/teme-2014-1049>.
- (57) Gottlieb, C.; Millar, S.; Grothe, S.; Wilsch, G. 2D Evaluation of Spectral LIBS Data Derived from Heterogeneous Materials Using Cluster Algorithm. *Spectrochim. Acta Part B At. Spectrosc.* **2017**, *134*, 58–68. <https://doi.org/10.1016/j.sab.2017.06.005>.
- (58) Taleb, A.; Motto-Ros, V.; Carru, M. J.; Axente, E.; Craciun, V.; Pelascini, F.; Hermann, J. Measurement Error Due to Self-Absorption in Calibration-Free Laser-Induced Breakdown Spectroscopy. *Anal. Chim. Acta* **2021**, *1185*, 339070. <https://doi.org/10.1016/j.aca.2021.339070>.
- (59) Bulajic, D.; Corsi, M.; Cristoforetti, G.; Legnaioli, S.; Palleschi, V.; Salvetti, A.; Tognoni, E. A Procedure for Correcting Self-Absorption in Calibration Free-Laser Induced Breakdown Spectroscopy. *Spectrochim. Acta Part B At. Spectrosc.* **2002**, *57* (2), 339–353. [https://doi.org/10.1016/S0584-8547\(01\)00398-6](https://doi.org/10.1016/S0584-8547(01)00398-6).
- (60) Li, J.; Hao, Z.; Zhao, N.; Zhou, R.; Yi, R.; Tang, S.; Guo, L.; Li, X.; Zeng, X.; Lu, Y. Spatially Selective Excitation in Laser-Induced Breakdown Spectroscopy Combined with Laser-Induced Fluorescence. *Opt. Express* **2017**, *25* (5), 4945–4951. <https://doi.org/10.1364/OE.25.004945>.
- (61) Darwiche, S.; Benmansour, M.; Eliezer, N.; Morvan, D. Laser-Induced Breakdown Spectroscopy for Photovoltaic Silicon Wafer Analysis. *Prog. Photovolt. Res. Appl.* **2012**, *20* (4), 463–471. <https://doi.org/10.1002/pip.1209>.
- (62) Quarles, C. D.; Gonzalez, J. J.; East, L. J.; Yoo, J. H.; Morey, M.; Russo, R. E. Fluorine Analysis Using Laser Induced Breakdown Spectroscopy (LIBS). *J. Anal. At. Spectrom.* **2014**, *29* (7), 1238–1242. <https://doi.org/10.1039/C4JA00061G>.
- (63) Syta, O.; Wagner, B.; Bulska, E.; Zielińska, D.; Żukowska, G. Z.; Gonzalez, J.; Russo, R. Elemental Imaging of Heterogeneous Inorganic Archaeological Samples by Means of Simultaneous

Laser Induced Breakdown Spectroscopy and Laser Ablation Inductively Coupled Plasma Mass Spectrometry Measurements. *Talanta* **2018**, *179*, 784–791.
<https://doi.org/10.1016/j.talanta.2017.12.011>.

(64) Cama-Moncunill, X.; Markiewicz-Keszycka, M.; Dixit, Y.; Cama-Moncunill, R.; Casado-Gavaldà, M. P.; Cullen, P. J.; Sullivan, C. Feasibility of Laser-Induced Breakdown Spectroscopy (LIBS) as an at-Line Validation Tool for Calcium Determination in Infant Formula. *Food Control* **2017**, *78*, 304–310.
<https://doi.org/10.1016/j.foodcont.2017.03.005>.

(65) Alombert-Goget, G.; Trichard, F.; Li, H.; Pezzani, C.; Silvestre, M.; Barthalay, N.; Motto-Ros, V.; Lebbou, K. Titanium Distribution Profiles Obtained by Luminescence and LIBS Measurements on Ti: Al₂O₃ Grown by Czochralski and Kyropoulos Techniques. *Opt. Mater.* **2017**, *65*, 28–32.
<https://doi.org/10.1016/j.optmat.2016.09.049>.

(66) Gimenez, Y.; Busser, B.; Trichard, F.; Kulesza, A.; Laurent, J. M.; Zaun, V.; Lux, F.; Benoit, J. M.; Panczer, G.; Dugourd, P.; Tillement, O.; Pelascini, F.; Sancey, L.; Motto-Ros, V. 3D Imaging of Nanoparticle Distribution in Biological Tissue by Laser-Induced Breakdown Spectroscopy. *Sci Rep* **2016**, *6*, 29936. <https://doi.org/10.1038/srep29936>.

(67) Trichard, F.; Sorbier, L.; Moncayo, S.; Blouët, Y.; Lienemann, C.-P.; Motto-Ros, V. Quantitative Elemental Imaging of Heterogeneous Catalysts Using Laser-Induced Breakdown Spectroscopy. *Spectrochim. Acta Part B At. Spectrosc.* **2017**, *133*, 45–51. <https://doi.org/10.1016/j.sab.2017.04.008>.

(68) Veber, P.; Bartosiewicz, K.; Debray, J.; Alombert-Goget, G.; Benamara, O.; Motto-Ros, V.; Thi, M. P.; Borta-Boyon, A.; Cabane, H.; Lebbou, K.; Levassort, F.; Kamada, K.; Yoshikawa, A.; Maglione, M. Lead-Free Piezoelectric Crystals Grown by the Micro-Pulling down Technique in the BaTiO₃–CaTiO₃–BaZrO₃ System. *CrystEngComm* **2019**, *21* (25), 3844–3853. <https://doi.org/10.1039/C9CE00405J>.

(69) Cugerone, A.; Cenki-Tok, B.; Oliot, E.; Muñoz, M.; Barou, F.; Motto-Ros, V.; Le Goff, E. Redistribution of Germanium during Dynamic Recrystallization of Sphalerite. *Geology* **2019**, *48* (3), 236–241. <https://doi.org/10.1130/G46791.1>.

(70) Cugerone, A.; Cenki-Tok, B.; Muñoz, M.; Kouzmanov, K.; Oliot, E.; Motto-Ros, V.; Le Goff, E. Behavior of Critical Metals in Metamorphosed Pb-Zn Ore Deposits: Example from the Pyrenean Axial Zone. *Miner. Deposita* **2021**, *56* (4), 685–705. <https://doi.org/10.1007/s00126-020-01000-9>.

(71) Sattmann, R.; Sturm, V.; Noll, R. Laser-Induced Breakdown Spectroscopy of Steel Samples Using Multiple Q-Switch Nd:YAG Laser Pulses. *J. Phys. Appl. Phys.* **1995**, *28* (10), 2181–2187.
<https://doi.org/10.1088/0022-3727/28/10/030>.

(72) Noll, R.; Fricke-Begemann, C.; Schreckenber, F. Laser-Induced Breakdown Spectroscopy as Enabling Key Methodology for Inverse Production of End-of-Life Electronics. *Spectrochim. Acta Part B At. Spectrosc.* **2021**, *181*, 106213. <https://doi.org/10.1016/j.sab.2021.106213>.

(73) Lee, S.-H.; Choi, J.-H.; In, J.-H.; Jeong, S. Fast Compositional Mapping of Solar Cell by Laser Spectroscopy Technique for Process Monitoring. *Int. J. Precis. Eng. Manuf.-Green Technol.* **2019**, *6* (2), 189–196. <https://doi.org/10.1007/s40684-019-00083-8>.

(74) Sdvizhenskii, P. A.; Lednev, V. N.; Grishin, M. Y.; Cheverikin, V. V.; Stavertiy, A. Y.; Tretyakov, R. S.; Asyutin, R. D.; Pershin, S. M. Laser Induced Breakdown Spectrometry for Elemental Mapping of Wear Resistant Coatings Synthesized by Laser Cladding. *J. Phys. Conf. Ser.* **2018**, *1109*, 012066.
<https://doi.org/10.1088/1742-6596/1109/1/012066>.

- (75) Weiss, M.; Gajarska, Z.; Lohninger, H.; Marchetti-Deschmann, M.; Ramer, G.; Lendl, B.; Limbeck, A. Elemental Mapping of Fluorine by Means of Molecular Laser Induced Breakdown Spectroscopy. *Anal. Chim. Acta* **2022**, *1195*, 339422. <https://doi.org/10.1016/j.aca.2021.339422>.
- (76) Agresti, J.; Indelicato, C.; Perotti, M.; Moreschi, R.; Osticioli, I.; Cacciari, I.; Mencaglia, A. A.; Siano, S. Quantitative Compositional Analyses of Calcareous Rocks for Lime Industry Using LIBS. *Molecules* **2022**, *27* (6), 1813. <https://doi.org/10.3390/molecules27061813>.
- (77) Veber, P.; Bartosiewicz, K.; Debray, J.; Pairis, S.; Motto-Ros, V.; Borta-Boyon, A.; Levassort, F.; Velazquez, M.; Vera, R.; Kamada, K.; Yoshikawa, A. Highly Textured Lead-Free Piezoelectric Polycrystals Grown by the Micro-Pulling down Freezing Technique in the BaTiO₃–CaTiO₃ System. *CrystEngComm* **2020**, *22* (30), 4982–4993. <https://doi.org/10.1039/D0CE00657B>.
- (78) Park, J.; Song, H.; Jang, I.; Lee, J.; Um, J.; Bae, S.; Kim, J.; Jeong, S.; Kim, H.-J. Three-Dimensionalization via Control of Laser-Structuring Parameters for High Energy and High Power Lithium-Ion Battery under Various Operating Conditions. *J. Energy Chem.* **2022**, *64*, 93–102. <https://doi.org/10.1016/j.jechem.2021.04.011>.
- (79) Grünberger, S.; Eschlböck-Fuchs, S.; Hofstadler, J.; Pissenberger, A.; Duchaczek, H.; Trautner, S.; Pedarnig, J. D. Analysis of Minor Elements in Steel and Chemical Imaging of Micro-Patterned Polymer by Laser Ablation-Spark Discharge-Optical Emission Spectroscopy and Laser-Induced Breakdown Spectroscopy. *Spectrochim. Acta Part B At. Spectrosc.* **2020**, *169*, 105884. <https://doi.org/10.1016/j.sab.2020.105884>.
- (80) Jolivet, L.; Motto-Ros, V.; Sorbier, L.; Sozinho, T.; Lienemann, C.-P. Quantitative Imaging of Carbon in Heterogeneous Refining Catalysts. *J. Anal. At. Spectrom.* **2020**, *35* (5), 896–903. <https://doi.org/10.1039/C9JA00434C>.
- (81) Trichard, F.; Gaulier, F.; Barbier, J.; Espinat, D.; Guichard, B.; Lienemann, C.-P.; Sorbier, L.; Levitz, P.; Motto-Ros, V. Imaging of Alumina Supports by Laser-Induced Breakdown Spectroscopy: A New Tool to Understand the Diffusion of Trace Metal Impurities. *J. Catal.* **2018**, *363*, 183–190. <https://doi.org/10.1016/j.jcat.2018.04.013>.
- (82) Jolivet, L.; Catita, L.; Delpoux, O.; Lienemann, C.-P.; Sorbier, L.; Motto-Ros, V. Direct Multi-Elemental Imaging of Freshly Impregnated Catalyst by Laser-Induced Breakdown Spectroscopy. *J. Catal.* **2021**, *401*, 183–187. <https://doi.org/10.1016/j.jcat.2021.07.010>.
- (83) Zhao, D.; Yi, R.; Eksaeva, A.; Oelmann, J.; Brezinsek, S.; Sergienko, G.; Rasinski, M.; Gao, Y.; Mayer, M.; Dhard, C. P.; Naujoks, D.; Cai, L.; and the W7-X Team. Quantification of Erosion Pattern Using Picosecond-LIBS on a Vertical Divertor Target Element Exposed in W7-X. *Nucl. Fusion* **2020**, *61* (1), 016025. <https://doi.org/10.1088/1741-4326/abc408>.
- (84) Yi, R.; Zhao, D.; Oelmann, J.; Brezinsek, S.; Rasinski, M.; Mayer, M.; Prakash Dhard, C.; Naujoks, D.; Liu, L.; Qu, J. 3-Dimensional Analysis of Layer Structured Samples with High Depth Resolution Using Picosecond Laser-Induced Breakdown Spectroscopy. *Appl. Surf. Sci.* **2020**, *532*, 147185. <https://doi.org/10.1016/j.apsusc.2020.147185>.
- (85) Choi, S.-U.; Han, S.-C.; Lee, J.-Y.; Yun, J.-I. Isotope Analysis of Iron on Structural Materials of Nuclear Power Plants Using Double-Pulse Laser Ablation Molecular Isotopic Spectrometry. *J. Anal. At. Spectrom.* **2021**, *36* (6), 1287–1296. <https://doi.org/10.1039/D1JA00097G>.

- (86) Zou, L.; Kassim, B.; Smith, J. P.; Ormes, J. D.; Liu, Y.; Tu, Q.; Bu, X. In Situ Analytical Characterization and Chemical Imaging of Tablet Coatings Using Laser Induced Breakdown Spectroscopy (LIBS). *Analyst* **2018**, *143* (20), 5000–5007. <https://doi.org/10.1039/C8AN01262H>.
- (87) Zou, L.; Stenslik, M. J.; Giles, M. B.; Ormes, J. D.; Marsales, M.; Santos, C.; Kassim, B.; Smith, J. P.; Gonzalez, J. J.; Bu, X. Direct Visualization of Drug Release in Injectable Implant by Laser Induced Breakdown Spectroscopy (LIBS). *J. Anal. At. Spectrom.* **2019**, *34* (7), 1351–1354. <https://doi.org/10.1039/C9JA00104B>.
- (88) Fabre, C.; Trebus, K.; Tarantola, A.; Cauzid, J.; Motto-Ros, V.; Voudouris, P. Advances on MicroLIBS and MicroXRF Mineralogical and Elemental Quantitative Imaging. *Spectrochim. Acta Part B At. Spectrosc.* **2022**, *194*, 106470. <https://doi.org/10.1016/j.sab.2022.106470>.
- (89) Mohamed, N.; Rifai, K.; Selmani, S.; Constantin, M.; Doucet, F. R.; Özcan, L. Ç.; Sabsabi, M.; Vidal, F. Chemical and Mineralogical Mapping of Platinum-Group Element Ore Samples Using Laser-Induced Breakdown Spectroscopy and Micro-X-Ray Fluorescence. *Geostand. Geoanalytical Res.* **2021**, *45* (3), 539–550. <https://doi.org/10.1111/ggr.12385>.
- (90) Raneri, S.; Botto, A.; Campanella, B.; Momčilović, M.; Palleschi, V.; Poggialini, F.; Sciuto, C.; Gattiglia, G.; Volpintesta, F.; Selvaraj, T.; Živković, S.; Lorenzetti, G.; Legnaioli, S. Increasing Resolution in Chemical Mapping of Geomaterials: From X-Ray Fluorescence to Laser-Induced Breakdown Spectroscopy. *Spectrochim. Acta Part B At. Spectrosc.* **2022**, *194*, 106482. <https://doi.org/10.1016/j.sab.2022.106482>.
- (91) Petit, J. R.; Jouzel, J.; Raynaud, D.; Barkov, N. I.; Barnola, J.-M.; Basile, I.; Bender, M.; Chappellaz, J.; Davis, M.; Delaygue, G.; Delmotte, M.; Kotlyakov, V. M.; Legrand, M.; Lipenkov, V. Y.; Lorius, C.; Pépin, L.; Ritz, C.; Saltzman, E.; Stievenard, M. Climate and Atmospheric History of the Past 420,000 Years from the Vostok Ice Core, Antarctica. *Nature* **1999**, *399* (6735), 429–436. <https://doi.org/10.1038/20859>.
- (92) Fairchild, I. J.; Treble, P. C. Trace Elements in Speleothems as Recorders of Environmental Change. *Quat. Sci. Rev.* **2009**, *28* (5–6), 449–468. <https://doi.org/10.1016/j.quascirev.2008.11.007>.
- (93) Hausmann, N.; Siozos, P.; Lemonis, A.; Colonese, A. C.; Robson, H. K.; Anglos, D. Elemental Mapping of Mg/Ca Intensity Ratios in Marine Mollusc Shells Using Laser-Induced Breakdown Spectroscopy. *J. Anal. At. Spectrom.* **2017**, *32* (8), 1467–1472. <https://doi.org/10.1039/C7JA00131B>.
- (94) Müller, S.; Meima, J. Mineral Classification of Lithium-Bearing Pegmatites Based on Laser-Induced Breakdown Spectroscopy: Application of Semi-Supervised Learning to Detect Known Minerals and Unknown Material. *Spectrochim. Acta Part B At. Spectrosc.* **2022**, *189*, 106370. <https://doi.org/10.1016/j.sab.2022.106370>.
- (95) Janovszky, P.; Jancsek, K.; Palásti, D. J.; Kopniczky, J.; Hopp, B.; Tóth, T. M.; Galbács, G. Classification of Minerals and the Assessment of Lithium and Beryllium Content in Granitoid Rocks by Laser-Induced Breakdown Spectroscopy. *J. Anal. At. Spectrom.* **2021**, *36* (4), 813–823. <https://doi.org/10.1039/D1JA00032B>.
- (96) Lawley, C. J. M.; Somers, A. M.; Kjarsgaard, B. A. Rapid Geochemical Imaging of Rocks and Minerals with Handheld Laser Induced Breakdown Spectroscopy (LIBS). *J. Geochem. Explor.* **2021**, *222*, 106694. <https://doi.org/10.1016/j.gexplo.2020.106694>.

- (97) Wise, M. A.; Harmon, R. S.; Curry, A.; Jennings, M.; Grimac, Z.; Khashchevskaya, D. Handheld LIBS for Li Exploration: An Example from the Carolina Tin-Spodumene Belt, USA. *Minerals* **2022**, *12* (1), 77. <https://doi.org/10.3390/min12010077>.
- (98) Gervais, F.; Rifai, K.; Plamondon, P.; Özcan, L.; Doucet, F.; Vidal, F. Compositional Tomography of a Gold-Bearing Sample by Laser-Induced Breakdown Spectroscopy. *Terra Nova* **2019**, *31* (5), 479–484. <https://doi.org/10.1111/ter.12417>.
- (99) Quarles, C. D.; Miao, T.; Poirier, L.; Gonzalez, J. J.; Lopez-Linares, F. Elemental Mapping and Characterization of Petroleum-Rich Rock Samples by Laser-Induced Breakdown Spectroscopy (LIBS). *Fuels* **2022**, *3* (2), 353–364. <https://doi.org/10.3390/fuels3020022>.
- (100) Rifai, K.; Ozcan, L.; Doucet, F.; Rhoderick, K.; Vidal, F. Ultrafast Elemental Mapping of Platinum Group Elements and Mineral Identification in Platinum-Palladium Ore Using Laser Induced Breakdown Spectroscopy. *Minerals* **2020**, *10*, 207. <https://doi.org/10.3390/min10030207>.
- (101) Fabre, C.; Devismes, D.; Moncayo, S.; Pelascini, F.; Trichard, F.; Lecomte, A.; Bousquet, B.; Cauzid, J.; Motto-Ros, V. Elemental Imaging by Laser-Induced Breakdown Spectroscopy for the Geological Characterization of Minerals. *J. Anal. At. Spectrom.* **2018**, *33* (8), 1345–1353. <https://doi.org/10.1039/C8JA00048D>.
- (102) Baele, J.-M.; BOUZAHZAH, H.; PAPIER, S.; Decrée, S.; Verheyden, S.; Burlet, C.; PIRARD, E.; FRANCESCHI, G.; DEJONGHE, L. Trace-Element Imaging at Macroscopic Scale in a Belgian Sphalerite-Galena Ore Using Laser-Induced Breakdown Spectroscopy (LIBS). *Geol. Belg.* **2021**, *24*, 125–136. <https://doi.org/10.20341/gb.2021.003>.
- (103) Müller, S.; Meima, J. A.; Rammilmair, D. Detecting REE-Rich Areas in Heterogeneous Drill Cores from Storkwitz Using LIBS and a Combination of k-Means Clustering and Spatial Raster Analysis. *J. Geochem. Explor.* **2021**, *221*, 106697. <https://doi.org/10.1016/j.gexplo.2020.106697>.
- (104) Gaft, M.; Raichlin, Y.; Pelascini, F.; Panzer, G.; Motto Ros, V. Imaging Rare-Earth Elements in Minerals by Laser-Induced Plasma Spectroscopy: Molecular Emission and Plasma-Induced Luminescence. *Spectrochim. Acta Part B At. Spectrosc.* **2019**, *151*, 12–19. <https://doi.org/10.1016/j.sab.2018.11.003>.
- (105) Holá, M.; Novotný, K.; Dobeš, J.; Kreml, I.; Wertich, V.; Mozola, J.; Kubeš, M.; Faltusová, V.; Leichmann, J.; Kanický, V. Dual Imaging of Uranium Ore by Laser Ablation Inductively Coupled Plasma Mass Spectrometry and Laser Induced Breakdown Spectroscopy. *Spectrochim. Acta Part B At. Spectrosc.* **2021**, *186*, 106312. <https://doi.org/10.1016/j.sab.2021.106312>.
- (106) Živković, S.; Botto, A.; Campanella, B.; Lezzerini, M.; Momčilović, M.; Pagnotta, S.; Palleschi, V.; Poggialini, F.; Legnaioli, S. Laser-Induced Breakdown Spectroscopy Elemental Mapping of the Construction Material from the Smederevo Fortress (Republic of Serbia). *Spectrochim. Acta Part B At. Spectrosc.* **2021**, *181*, 106219. <https://doi.org/10.1016/j.sab.2021.106219>.
- (107) Nardecchia, A.; de Juan, A.; Motto-Ros, V.; Gaft, M.; Duponchel, L. Data Fusion of LIBS and PIL Hyperspectral Imaging: Understanding the Luminescence Phenomenon of a Complex Mineral Sample. *Anal. Chim. Acta* **2022**, *1192*, 339368. <https://doi.org/10.1016/j.aca.2021.339368>.
- (108) Trejos, T.; Vander Pyl, C.; Menking-Hoggatt, K.; Alvarado, A. L.; Arroyo, L. E. Fast Identification of Inorganic and Organic Gunshot Residues by LIBS and Electrochemical Methods. *Forensic Chem.* **2018**, *8*, 146–156. <https://doi.org/10.1016/j.forc.2018.02.006>.

- (109) Naozuka, J.; Oliveira, A. P. CHAPTER 4 Laser-Induced Breakdown Spectroscopy (LIBS) in Forensic Sensing. In *Forensic Analytical Methods*; The Royal Society of Chemistry, 2019; pp 48–78. <https://doi.org/10.1039/9781788016117-00048>.
- (110) Pyl, C. V.; Ovide, O.; Ho, M.; Yuksel, B.; Trejos, T. Spectrochemical Mapping Using Laser Induced Breakdown Spectroscopy as a More Objective Approach to Shooting Distance Determination. *Spectrochim. Acta Part B At. Spectrosc.* **2019**, *152*, 93–101. <https://doi.org/10.1016/j.sab.2018.12.010>.
- (111) Mistek, E.; Fikiet, M. A.; Khandasammy, S. R.; Lednev, I. K. Toward Locard's Exchange Principle: Recent Developments in Forensic Trace Evidence Analysis. *Anal. Chem.* **2019**, *91* (1), 637–654. <https://doi.org/10.1021/acs.analchem.8b04704>.
- (112) Yang, J.-H.; Choi, S.-J.; Yoh, J. J. Towards Reconstruction of Overlapping Fingerprints Using Plasma Spectroscopy. *Spectrochim. Acta Part B At. Spectrosc.* **2017**, *134*, 25–32. <https://doi.org/10.1016/j.sab.2017.06.001>.
- (113) Yang, J.-H.; Yoh, J. J. Reconstruction of Chemical Fingerprints from an Individual's Time-Delayed, Overlapped Fingerprints via Laser-Induced Breakdown Spectrometry (LIBS) and Raman Spectroscopy. *Microchem. J.* **2018**, *139*, 386–393. <https://doi.org/10.1016/j.microc.2018.03.027>.
- (114) Hilario, F. F.; Mello, M. L. de; Pereira-Filho, E. R. Forensic Analysis of Hand-Written Documents Using Laser-Induced Breakdown Spectroscopy (LIBS) and Chemometrics. *Anal. Methods* **2021**, *13* (2), 232–241. <https://doi.org/10.1039/D0AY02089C>.
- (115) Yin, P.; Yang, E.; Chen, Y.; Peng, Z.; Li, D.; Duan, Y.; Lin, Q. Multiplexing Steganography Based on Laser-Induced Breakdown Spectroscopy Coupled with Machine Learning. *Chem. Commun.* **2021**, *57* (59), 7312–7315. <https://doi.org/10.1039/D1CC02787E>.
- (116) Moncayo, S.; Trichard, F.; Busser, B.; Sabatier-Vincent, M.; Pelascini, F.; Pinel, N.; Templier, I.; Charles, J.; Sancey, L.; Motto-Ros, V. Multi-Elemental Imaging of Paraffin-Embedded Human Samples by Laser-Induced Breakdown Spectroscopy. *Spectrochim. Acta Part B At. Spectrosc.* **2017**, *133*, 40–44. <https://doi.org/10.1016/j.sab.2017.04.013>.
- (117) Busser, B.; Moncayo, S.; Trichard, F.; Bonnetterre, V.; Pinel, N.; Pelascini, F.; Dugourd, P.; Coll, J. L.; D'Incan, M.; Charles, J.; Motto-Ros, V.; Sancey, L. Characterization of Foreign Materials in Paraffin-Embedded Pathological Specimens Using in Situ Multi-Elemental Imaging with Laser Spectroscopy. *Mod Pathol* **2018**, *31* (3), 378–384. <https://doi.org/10.1038/modpathol.2017.152>.
- (118) Modlitbová, P.; Pořízka, P.; Kaiser, J. Laser-Induced Breakdown Spectroscopy as a Promising Tool in the Elemental Bioimaging of Plant Tissues. *TrAC Trends Anal. Chem.* **2020**, *122*, 115729. <https://doi.org/10.1016/j.trac.2019.115729>.
- (119) Ilhardt, P. D.; Nuñez, J. R.; Denis, E. H.; Rosnow, J. J.; Krogstad, E. J.; Renslow, R. S.; Moran, J. J. High-Resolution Elemental Mapping of the Root-Rhizosphere-Soil Continuum Using Laser-Induced Breakdown Spectroscopy (LIBS). *Soil Biol. Biochem.* **2019**, *131*, 119–132. <https://doi.org/10.1016/j.soilbio.2018.12.029>.
- (120) de Oliveira, A. P.; de Oliveira Leme, F.; Nomura, C. S.; Naozuka, J. Elemental Imaging by Laser-Induced Breakdown Spectroscopy to Evaluate Selenium Enrichment Effects in Edible Mushrooms. *Sci. Rep.* **2019**, *9* (1), 10827. <https://doi.org/10.1038/s41598-019-47338-7>.

- (121) Singh, V. K.; Tripathi, D. K.; Mao, X.; Russo, R. E.; Zorba, V. Elemental Mapping of Lithium Diffusion in Doped Plant Leaves Using Laser-Induced Breakdown Spectroscopy (LIBS). *Appl. Spectrosc.* **2019**, *73* (4), 387–394. <https://doi.org/10.1177/0003702819830394>.
- (122) Peng, J.; He, Y.; Zhao, Z.; Jiang, J.; Zhou, F.; Liu, F.; Shen, T. Fast Visualization of Distribution of Chromium in Rice Leaves by Re-Heating Dual-Pulse Laser-Induced Breakdown Spectroscopy and Chemometric Methods. *Environ. Pollut.* **2019**, *252*, 1125–1132. <https://doi.org/10.1016/j.envpol.2019.06.027>.
- (123) Dell'Aglio, M.; Alrifai, R.; De Giacomo, A. Nanoparticle Enhanced Laser Induced Breakdown Spectroscopy (NELIBS), a First Review. *Spectrochim. Acta Part B At. Spectrosc.* **2018**, *148*, 105–112. <https://doi.org/10.1016/j.sab.2018.06.008>.
- (124) Zhao, X.; Zhao, C.; Du, X.; Dong, D. Detecting and Mapping Harmful Chemicals in Fruit and Vegetables Using Nanoparticle-Enhanced Laser-Induced Breakdown Spectroscopy. *Sci. Rep.* **2019**, *9* (1), 906. <https://doi.org/10.1038/s41598-018-37556-w>.
- (125) Modlitbová, P.; Pořízka, P.; Střítežská, S.; Zezulka, Š.; Kummerová, M.; Novotný, K.; Kaiser, J. Detail Investigation of Toxicity, Bioaccumulation, and Translocation of Cd-Based Quantum Dots and Cd Salt in White Mustard. *Chemosphere* **2020**, *251*, 126174. <https://doi.org/10.1016/j.chemosphere.2020.126174>.
- (126) Le Guevel, X.; Henry, M.; Motto-Ros, V.; Longo, E.; Montanez, M. I.; Pelascini, F.; de La Rochefoucauld, O.; Zeitoun, P.; Coll, J. L.; Josserand, V.; Sancey, L. Elemental and Optical Imaging Evaluation of Zwitterionic Gold Nanoclusters in Glioblastoma Mouse Models. *Nanoscale* **2018**, *10* (39), 18657–18664. <https://doi.org/10.1039/c8nr05299a>.
- (127) Busser, B.; Bulin, A.-L.; Gardette, V.; Elleaume, H.; Pelascini, F.; Bouron, A.; Motto-Ros, V.; Sancey, L. Visualizing the Cerebral Distribution of Chemical Elements: A Challenge Met with LIBS Elemental Imaging. *J. Neurosci. Methods* **2022**, *379*, 109676. <https://doi.org/10.1016/j.jneumeth.2022.109676>.
- (128) Meng, Y.; Gao, C.; Lin, Z.; Hang, W.; Huang, B. Nanoscale Laser-Induced Breakdown Spectroscopy Imaging Reveals Chemical Distribution with Subcellular Resolution. *Nanoscale Adv.* **2020**, *2* (9), 3983–3990. <https://doi.org/10.1039/D0NA00380H>.
- (129) Galbács, G.; Kéri, A.; Kohut, A.; Veres, M.; Geretovszky, Zs. Nanoparticles in Analytical Laser and Plasma Spectroscopy – a Review of Recent Developments in Methodology and Applications. *J. Anal. At. Spectrom.* **2021**, *36* (9), 1826–1872. <https://doi.org/10.1039/D1JA00149C>.
- (130) Hartnell, D.; Andrews, W.; Smith, N.; Jiang, H.; McAllum, E.; Rajan, R.; Colbourne, F.; Fitzgerald, M.; Lam, V.; Takechi, R.; Pushie, M. J.; Kelly, M. E.; Hackett, M. J. A Review of Ex Vivo Elemental Mapping Methods to Directly Image Changes in the Homeostasis of Diffusible Ions (Na⁺, K⁺, Mg²⁺, Ca²⁺, Cl⁻) Within Brain Tissue. *Front. Neurosci.* **2020**, *13*, 1415. <https://doi.org/10.3389/fnins.2019.01415>.
- (131) Lin, Q.; Wang, S.; Duan, Y.; Tuchin, V. V. Ex Vivo Three-Dimensional Elemental Imaging of Mouse Brain Tissue Block by Laser-Induced Breakdown Spectroscopy. *J. Biophotonics* **2021**, *14* (5), e202000479. <https://doi.org/10.1002/jbio.202000479>.
- (132) Bulin, A.-L.; Broekgaarden, M.; Chaput, F.; Baisamy, V.; Garrevoet, J.; Busser, B.; Brueckner, D.; Youssef, A.; Ravanat, J.-L.; Dujardin, C.; Motto-Ros, V.; Lerouge, F.; Bohic, S.; Sancey, L.; Elleaume, H. Radiation Dose-Enhancement Is a Potent Radiotherapeutic Effect of Rare-Earth Composite

Nanoscintillators in Preclinical Models of Glioblastoma. *Adv. Sci.* **2020**, *7* (20), 2001675.
<https://doi.org/10.1002/advs.202001675>.

(133) Kalot, G.; Godard, A.; Busser, B.; Pliquett, J.; Broekgaarden, M.; Motto-Ros, V.; Wegner, K. D.; Resch-Genger, U.; Köster, U.; Denat, F.; Coll, J.-L.; Bodio, E.; Goze, C.; Sancey, L. Aza-BODIPY: A New Vector for Enhanced Theranostic Boron Neutron Capture Therapy Applications. *Cells* **2020**, *9* (9), 1953. <https://doi.org/10.3390/cells9091953>.

(134) Manard, B. T.; Hintz, C. J.; Quarles, C. D.; Burns, W.; Ziraqparvar, N. A.; Dunlap, D. R.; Beiswenger, T.; Cruz-Uribe, A. M.; Petrus, J. A.; Hexel, C. R. Determination of Fluorine Distribution in Shark Teeth by Laser-Induced Breakdown Spectroscopy. *Metallomics* **2022**, *14* (7), mfac050.
<https://doi.org/10.1093/mtomcs/mfac050>.

(135) Xu, F.; Ma, S.; Zhao, C.; Dong, D. Application of Molecular Emissions in Laser-Induced Breakdown Spectroscopy: A Review. *Front. Phys.* **2022**, *10*, 7.
<https://doi.org/10.3389/fphy.2022.821528>.

(136) Choi, J.-H.; Shin, S.; Moon, Y.; Han, J.; Hwang, E.; Jeong, S. High Spatial Resolution Imaging of Melanoma Tissue by Femtosecond Laser-Induced Breakdown Spectroscopy. *Spectrochim. Acta Part B At. Spectrosc.* **2021**, *179*, 106090. <https://doi.org/10.1016/j.sab.2021.106090>.

(137) Kiss, K.; Šindelářová, A.; Krbal, L.; Stejskal, V.; Mrázová, K.; Vrábel, J.; Kaška, M.; Modlitbová, P.; Pořízka, P.; Kaiser, J. Imaging Margins of Skin Tumors Using Laser-Induced Breakdown Spectroscopy and Machine Learning. *J. Anal. At. Spectrom.* **2021**, *36* (5), 909–916.
<https://doi.org/10.1039/D0JA00469C>.

(138) WMA - The World Medical Association-WMA Declaration of Helsinki – Ethical Principles for Medical Research Involving Human Subjects. <https://www.wma.net/policies-post/wma-declaration-of-helsinki-ethical-principles-for-medical-research-involving-human-subjects/> (accessed 2022-11-01).

(139) Khan, M. N.; Wang, Q.; Idrees, B. S.; Xiangli, W.; Teng, G.; Cui, X.; Zhao, Z.; Wei, K.; Abrar, M. A Review on Laser-Induced Breakdown Spectroscopy in Different Cancers Diagnosis and Classification. *Front. Phys.* **2022**, *10*, 821057. <https://doi.org/10.3389/fphy.2022.821057>.

(140) Yin, P.; Hu, B.; Li, Q.; Duan, Y.; Lin, Q. Imaging of Tumor Boundary Based on Multielements and Molecular Fragments Heterogeneity in Lung Cancer. *IEEE Trans. Instrum. Meas.* **2021**, *70*, 1–7.
<https://doi.org/10.1109/TIM.2021.3102755>.

(141) University Hospital, Grenoble. *Multi-Elemental Imaging of Lung Tissues With LIBS (Laser-Induced Breakdown Spectroscopy) : A Feasibility Study*; Clinical trial registration NCT03901196; clinicaltrials.gov, 2022. <https://clinicaltrials.gov/ct2/show/NCT03901196> (accessed 2022-08-31).

(142) Martinez, M.; Baudelet, M. Calibration Strategies for Elemental Analysis of Biological Samples by LA-ICP-MS and LIBS – A Review. *Anal. Bioanal. Chem.* **2020**, *412* (1), 27–36.
<https://doi.org/10.1007/s00216-019-02195-1>.

(143) Legnaioli, S.; Campanella, B.; Pagnotta, S.; Poggialini, F.; Palleschi, V. Chapter 24 - Self-Calibrated Methods for LIBS Quantitative Analysis. In *Laser-Induced Breakdown Spectroscopy (Second Edition)*; Singh, J. P., Thakur, S. N., Eds.; Elsevier: Amsterdam, 2020; pp 561–580.
<https://doi.org/10.1016/B978-0-12-818829-3.00024-1>.

- (144) Motto-Ros, V.; Moncayo, S.; Trichard, F.; Pelascini, F. Investigation of Signal Extraction in the Frame of Laser Induced Breakdown Spectroscopy Imaging. *Spectrochim. Acta Part B At. Spectrosc.* **2019**, *155*, 127–133. <https://doi.org/10.1016/j.sab.2019.04.004>.
- (145) Nardecchia, A.; Motto-Ros, V.; Duponchel, L. Saturated Signals in Spectroscopic Imaging: Why and How Should We Deal with This Regularly Observed Phenomenon? *Anal. Chim. Acta* **2021**, *1157*, 338389. <https://doi.org/10.1016/j.aca.2021.338389>.
- (146) Richiero, S.; Sandoval, C.; Oberlin, C.; Schmitt, A.; Lefevre, J.-C.; Bensalah-Ledoux, A.; Prigent, D.; Coquidé, C.; Valois, A.; Giletti, F.; Pelascini, F.; Duponchel, L.; Dugourd, P.; Comby-Zerbino, C.; Motto-Ros, V. Archaeological Mortar Characterization Using Laser-Induced Breakdown Spectroscopy (LIBS) Imaging Microscopy. *Appl. Spectrosc.* **2022**, *76* (8), 978–987. <https://doi.org/10.1177/00037028211071141>.
- (147) Moncayo, S.; Duponchel, L.; Mousavipak, N.; Panczer, G.; Trichard, F.; Bousquet, B.; Pelascini, F.; Motto-Ros, V. Exploration of Megapixel Hyperspectral LIBS Images Using Principal Component Analysis. *J. Anal. At. Spectrom.* **2018**, *33* (2), 210–220. <https://doi.org/10.1039/C7JA00398F>.
- (148) Finotello, R.; Tamaazousti, M.; Sirven, J.-B. HyperPCA: A Powerful Tool to Extract Elemental Maps from Noisy Data Obtained in LIBS Mapping of Materials. *Spectrochim. Acta Part B At. Spectrosc.* **2022**, *192*, 106418. <https://doi.org/10.1016/j.sab.2022.106418>.
- (149) Nardecchia, A.; Fabre, C.; Cauzid, J.; Pelascini, F.; Motto-Ros, V.; Duponchel, L. Detection of Minor Compounds in Complex Mineral Samples from Millions of Spectra: A New Data Analysis Strategy in LIBS Imaging. *Anal. Chim. Acta* **2020**, *1114*, 66–73. <https://doi.org/10.1016/j.aca.2020.04.005>.
- (150) Wu, Q.; Marina-Montes, C.; Cáceres, J. O.; Anzano, J.; Motto-Ros, V.; Duponchel, L. Interesting Features Finder (IFF): Another Way to Explore Spectroscopic Imaging Data Sets Giving Minor Compounds and Traces a Chance to Express Themselves. *Spectrochim. Acta Part B At. Spectrosc.* **2022**, *195*, 106508. <https://doi.org/10.1016/j.sab.2022.106508>.
- (151) Meima, J. A.; Rammlair, D. Investigation of Compositional Variations in Chromitite Ore with Imaging Laser Induced Breakdown Spectroscopy and Spectral Angle Mapper Classification Algorithm. *Chem. Geol.* **2020**, *532*, 119376. <https://doi.org/10.1016/j.chemgeo.2019.119376>.
- (152) Müller, S.; Meima, J. A. Mineral Classification of Lithium-Bearing Pegmatites Based on Laser-Induced Breakdown Spectroscopy: Application of Semi-Supervised Learning to Detect Known Minerals and Unknown Material. *Spectrochim. Acta Part B At. Spectrosc.* **2022**, *189*, 106370. <https://doi.org/10.1016/j.sab.2022.106370>.
- (153) Choi, J.-H.; Shin, S.; Moon, Y.; Han, J. H.; Hwang, E.; Jeong, S. High Spatial Resolution Imaging of Melanoma Tissue by Femtosecond Laser-Induced Breakdown Spectroscopy. *Spectrochim. Acta Part B At. Spectrosc.* **2021**, *179*, 106090. <https://doi.org/10.1016/j.sab.2021.106090>.
- (154) Casado-Gavalda, M. P.; Dixit, Y.; Geulen, D.; Cama-Moncunill, R.; Cama-Moncunill, X.; Markiewicz-Keszycska, M.; Cullen, P. J.; Sullivan, C. Quantification of Copper Content with Laser Induced Breakdown Spectroscopy as a Potential Indicator of Offal Adulteration in Beef. *Talanta* **2017**, *169*, 123–129. <https://doi.org/10.1016/j.talanta.2017.03.071>.
- (155) Dixit, Y.; Casado-Gavalda, M. P.; Cama-Moncunill, R.; Cama-Moncunill, X.; Markiewicz-Keszycska, M.; Cullen, P. J.; Sullivan, C. Laser Induced Breakdown Spectroscopy for Quantification of

Sodium and Potassium in Minced Beef: A Potential Technique for Detecting Beef Kidney Adulteration. *Anal. Methods* **2017**, *9* (22), 3314–3322. <https://doi.org/10.1039/C7AY00757D>.

(156) Cama-Moncunill, X.; Markiewicz-Keszycka, M.; Dixit, Y.; Cama-Moncunill, R.; Casado-Gavaldà, M. P.; Cullen, P. J.; Sullivan, C. Feasibility of Laser-Induced Breakdown Spectroscopy (LIBS) as an at-Line Validation Tool for Calcium Determination in Infant Formula. *Food Control* **2017**, *78*, 304–310. <https://doi.org/10.1016/j.foodcont.2017.03.005>.

(157) Sandoval-Muñoz, C.; Velásquez, G.; Álvarez, J.; Pérez, F.; Velásquez, M.; Torres, S.; Sbarbaro-Hofer, D.; Motto-Ros, V.; Yáñez, J. Enhanced Elemental and Mineralogical Imaging of Cu-Mineralized Rocks by Coupling μ -LIBS and HSI. *J. Anal. At. Spectrom.* **2022**, *37* (10), 1981–1993. <https://doi.org/10.1039/D2JA00147K>.

(158) El Haddad, J.; de Lima Filho, E. S.; Vanier, F.; Harhira, A.; Padioleau, C.; Sabsabi, M.; Wilkie, G.; Blouin, A. Multiphase Mineral Identification and Quantification by Laser-Induced Breakdown Spectroscopy. *Miner. Eng.* **2019**, *134*, 281–290. <https://doi.org/10.1016/j.mineng.2019.02.025>.

(159) Nardecchia, A.; de Juan, A.; Motto-Ros, V.; Gaft, M.; Duponchel, L. Data Fusion of LIBS and PIL Hyperspectral Imaging: Understanding the Luminescence Phenomenon of a Complex Mineral Sample. *Anal. Chim. Acta* **2022**, *1192*, 339368. <https://doi.org/10.1016/j.aca.2021.339368>.

(160) Pagnotta, S.; Lezzerini, M.; Ripoll-Seguer, L.; Hidalgo, M.; Grifoni, E.; Legnaioli, S.; Lorenzetti, G.; Poggialini, F.; Palleschi, V. Micro-Laser-Induced Breakdown Spectroscopy (Micro-LIBS) Study on Ancient Roman Mortars. *Appl. Spectrosc.* **2017**, *71* (4), 721–727. <https://doi.org/10.1177/0003702817695289>.

(161) Pagnotta, S.; Lezzerini, M.; Campanella, B.; Gallelo, G.; Grifoni, E.; Legnaioli, S.; Lorenzetti, G.; Poggialini, F.; Raneri, S.; Safi, A.; Palleschi, V. Fast Quantitative Elemental Mapping of Highly Inhomogeneous Materials by Micro-Laser-Induced Breakdown Spectroscopy. *Spectrochim. Acta Part B At. Spectrosc.* **2018**, *146*, 9–15. <https://doi.org/10.1016/j.sab.2018.04.018>.

(162) Chen, T.; Sun, L.; Yu, H.; Wang, W.; Qi, L.; Zhang, P.; Zeng, P. Deep Learning with Laser-Induced Breakdown Spectroscopy (LIBS) for the Classification of Rocks Based on Elemental Imaging. *Appl. Geochem.* **2022**, *136*, 105135. <https://doi.org/10.1016/j.apgeochem.2021.105135>.

(163) Gaft, M.; Nagli, L.; Raichlin, Y.; Pelascini, F.; Panzer, G.; Ros, V. M. Laser-Induced Breakdown Spectroscopy of Br and I Molecules with Alkali-Earth Elements. *Spectrochim. Acta Part B At. Spectrosc.* **2019**, *157*, 47–52. <https://doi.org/10.1016/j.sab.2019.05.003>.

(164) Gaft, M.; Nagli, L.; Gornushkin, I.; Raichlin, Y. Review on Recent Advances in Analytical Applications of Molecular Emission and Modelling. *Spectrochim. Acta Part B At. Spectrosc.* **2020**, *173*, 105989. <https://doi.org/10.1016/j.sab.2020.105989>.

(165) Clavé, E.; Gaft, M.; Motto-Ros, V.; Fabre, C.; Forni, O.; Beyssac, O.; Maurice, S.; Wiens, R. C.; Bousquet, B. Extending the Potential of Plasma-Induced Luminescence Spectroscopy. *Spectrochim. Acta Part B At. Spectrosc.* **2021**, *177*, 106111. <https://doi.org/10.1016/j.sab.2021.106111>.